Chapter 4

Investigating the Influence of Different Types of Nanoparticles on Thermal and Dielectric Properties of Insulation in Converter Transformer

Boxue Du

Additional information is available at the end of the chapter

http://dx.doi.org/10.5772/67432

Abstract

Converter transformer is the extraordinarily vital apparatus in the high-voltage direct current (HVDC). Transformer oil and oil-impregnated paper are considered as the essential parts of converter transformer, which has suffered various complex electric fields such as AC/DC composite electric field and polarity reversal. The occurrence of discharge or insulation failure in oil-paper insulation system will threaten the safety of the entire grid. Hence, efforts should be focused on investigating the charge behavior and improving the property of dielectric.

This chapter presents a study aimed at investigating the influence of different types of nanoparticles on thermal and dielectric properties along with the relation between them and the effects of switching overvoltage on the charge coupling behavior of oil-impregnated paper, and the surface charge behavior on double-layer oil-paper insulation under pulse voltage is investigated.

Keywords: converter transformer, oil-impregnated paper, nanoparticles, thermal conductivity, operation overvoltage, surface charge

1. Introduction

In recent years, the utilization of an HVDC system is becoming an inevitable trend with the developments in the worldwide power industry and improvements in voltage levels [1–3]. Meanwhile, oil-paper insulation has been widely used in converter transformers as well as HVDC bushings, and its safety is closely related to the security of large power transformers even the entire grid. Usually, oil-paper insulation withstands DC voltage under normal conditions. When extreme states appear, it will be subjected to various overvoltages, and the overvoltage will cause the rise of the electric field of the oil-paper insulation in a short time. Operating impulse voltage is a kind of overvoltage that often occurs in converter transformers and HVDC bushings. For example, the switching of thyristors often appears in power electronic equipment, and overvoltage has a cumulative and repeated effect on oil-paper insulation damage. So, it is necessary to study the effects of operating overvoltage on oil-paper insulation. Actually, charge accumulation under overvoltage is one of the main reasons that cause aging and breakdown of oil-paper insulation. But the effect of operating overvoltage on the charge injection and dissipation is still unclear. Current researches mainly focus on effects of lightning pulse voltage on oil-paper insulation, but for operating overvoltage, the influence of its cumulative effect on oil-paper insulation needs further investigation. Furthermore, how DC and pulse voltages affect charge coupling of oil-paper insulation calls for more consideration and investigation.

Furthermore, the mineral oil applied in transformers fills up the pores in the fibrous insulation and performs dual functions of insulating materials and effective coolant. For thermal property, the oil carries away the heat generated during normal operation by conduction and convection [4]. Moreover, the oil can affect the dielectric property of oil-paper insulation system and thus influence the breakdown strength of the transformers. New type of transformer oil with enhanced dielectric property and thermal conductivity is in urgent need with the miniaturization and high voltage of electric devices processing. Most studies on nano-modified transformer oil were limited to the dielectric property or thermal property. Very few researchers considered investigating the relation between the thermal property and the dielectric breakdown strength. In this chapter, Boron nitride (BN) nanoparticles with high thermal conductivity and ferriferrous oxide (Fe_3O_4) nanoparticles as a typical magnetic oxide were dispersed into transformer oil to form different types of nanooil. Thermal properties including thermal conductivity and thermal diffusivity were measured with varying the mass fraction and temperature. Dielectric properties and breakdown strength under different temperature were measured to investigate the influence of temperature on the nanooil.

Therefore, this chapter will focus on the investigating the influence of different types of nanoparticles on thermal and dielectric properties along with the relation between them and the effects of different application conditions on surface charge behavior of oil-paper insulation to understand and analyze the transportation of charge in the oil-paper insulation and the effects of voltage amplitude, pulse frequency, numbers as well as polarity on the charge accumulation and dissipation.

http://dx.doi.org/10.5772/67432

2. Thermal conductivity and dielectric characteristics of transformer oil filled with BN and Fe_3O_4 nanoparticles

2.1. Experiments

In this research, the average grain diameter and surface to volume of the BN nanoparticles are 50 nm and 43.6 m^2/g, while they are 20 nm and 66 m^2/g for the Fe_3O_4 nanoparticles. The nanoparticles were dried to decrease the adsorbed water content before dispersion. The transformer oil used was purified through a vacuum oil filter. The two types of nanoparticles with the mass fraction of 0.05, 0.1 wt% were dispersed into the filtered oil by a stirrer and ultrasonic vibrated to promote dispersion and reduce possible agglomeration. All the samples were degassed before measurements. The nanoparticles were dispersed uniformly in the base oil.

2.2. Effect on thermal conductivity

The THW method is employed to measure the thermal parameters. Thermal conductivity of the two types of nanooil and the pure oil is shown in **Figure 1**. The nanooil with BN nanoparticles shows more obvious enhancement compared to the oil dispersed with Fe_3O_4 nanoparticles under the same mass fraction and temperature. The BN-modified nanooil at the mass fraction of 0.05 wt% reaches the thermal conductivity of 0.1184 W m^{-1} K^{-1} when the applied

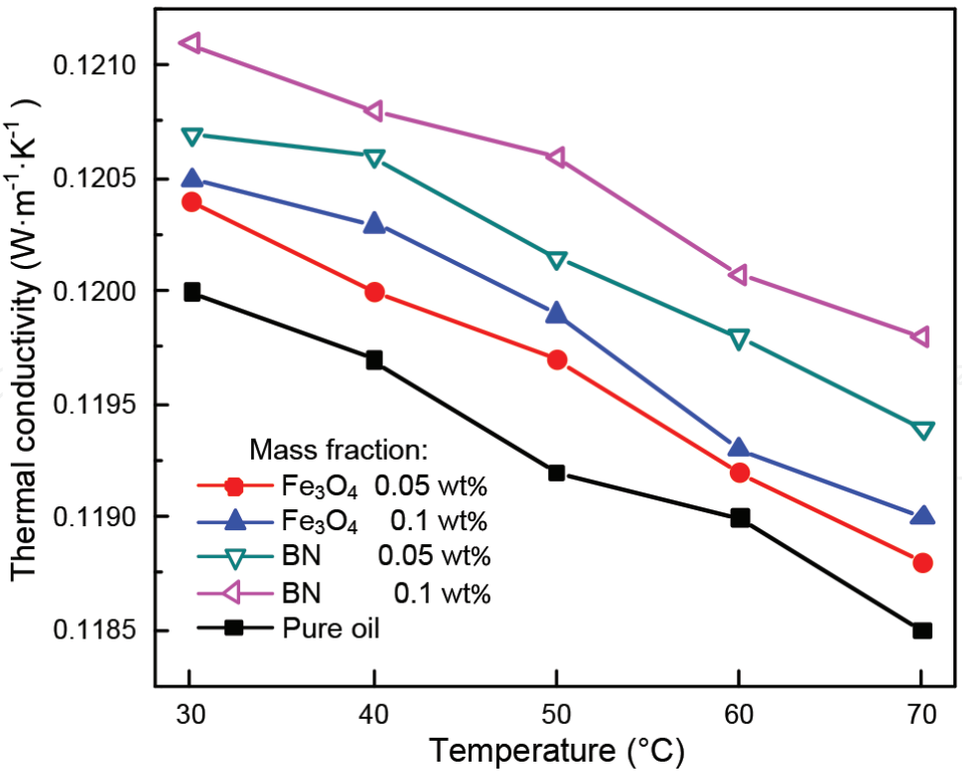

Figure 1. Relation between the thermal conductivity and the temperature with the different mass fractions.

temperature is 70°C which is even higher than the oil modified with Fe_3O_4 nanoparticles at the mass fraction of 0.1%. Thermal conductivity increases with increasing the mass fraction and decreases with increasing temperature for each type of the nanooil. The thermal conductivity shows linear decline tendency in the variation of temperature as measured.

It is considered that the interfacial region due to the addition of nanoparticles and the ballistic phonon transport among nanoparticles contribute to the considerable improvement. The liquid molecules close to the nanoparticles form a nanolayer which functions as a bridge linking the additional nanoparticles and the liquid molecules, thus causing the increase of thermal conductivity [5]. Moreover, Keblinski presented a ballistic phonon transport theory that the ballistic phonons originated in one particle can spread to an adjacent particle and contribute to the remarkable enhancement much compared to Brownian motion even at extremely low mass fraction [6]. The higher thermal conductivity of the BN-modified oil compared with the Fe_3O_4-modified oil is expected to attribute to the higher thermal conductivity of BN nanoparticles.

Figure 2 shows the temperature-dependent thermal diffusivity of the pure oil and the nanooil modified with BN and Fe_3O_4 nanoparticles, respectively. With the mass fraction of 0.1%, the increase in thermal diffusivity is observed to be 8.7% for the BN-modified oil and 2.6% for the Fe_3O_4-modified oil at the temperature of 30°C, respectively. As shown in **Figure 2**, the thermal diffusivity of the oil performs nearly the same decline slope with varying the temperature

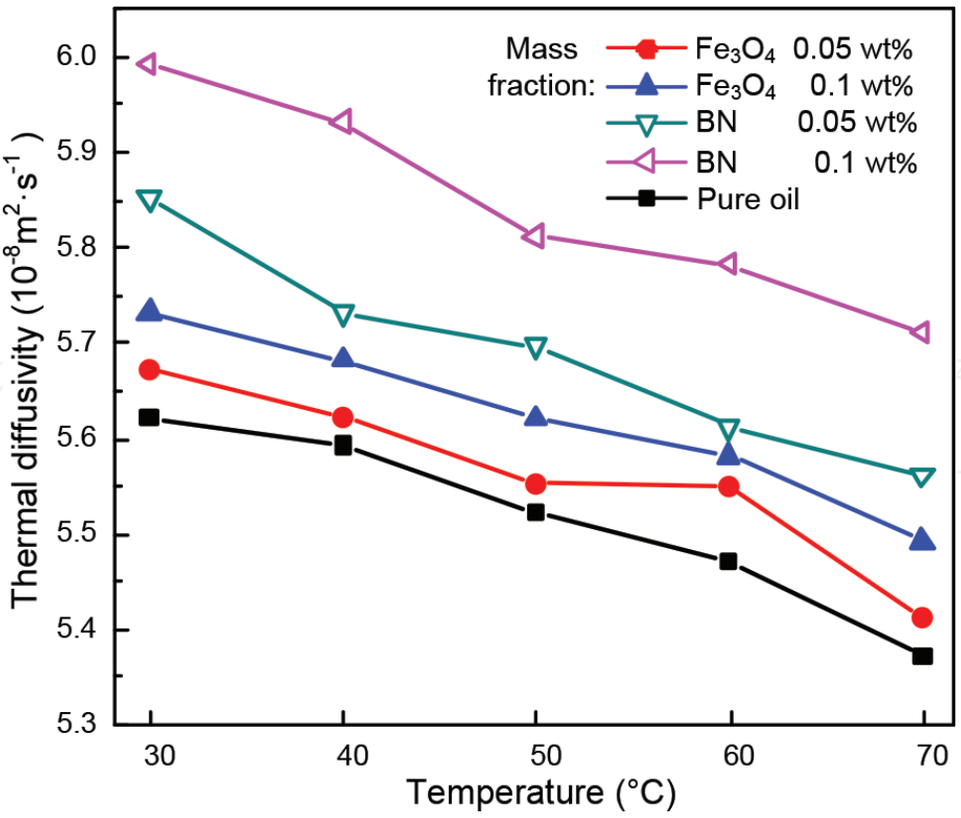

Figure 2. Relation between the thermal diffusivity and the temperature with the different mass fractions.

http://dx.doi.org/10.5772/67432

indicating slight influence of the nanoparticles on temperature-dependent thermal diffusivity in the range of present concentrations.

The improvement in thermal diffusivity is considered to be due to the enhanced thermal conductivity as shown in **Figure 1** which varies with the mass fraction. Moreover, with increasing the loading of nanoparticles, the specific heat decreases as shown in **Figure 3** which leads to an increase in thermal diffusivity as mentioned by Murshed et al. [7]. Furthermore, due to the high thermal conductivity of BN nanoparticles, the thermal diffusivity of the BN-modified oil achieves more obvious enhancement in comparison with the Fe_3O_4-modified oil.

Figure 3 illustrates the effect of nanoparticles on the specific heat with different mass fractions. The specific heat decreases with increasing the mass fraction for each type of the nanooil showing the opposite tendency in thermal conductivity and thermal diffusivity tests. The mechanism for the decline of specific heat when introduced with nanoparticles should attribute to the much smaller specific heat of the nanoparticles compared to the base oil [8]. The result also shows that the oil modified with Fe_3O_4 nanoparticles obtains higher specific heat at the same mass fraction in contrast with the BN-modified oil.

The temperature change of the coil in heating process is given in **Figure 4**. The transformer oil modified with BN and Fe_3O_4 nanoparticles at the mass fraction of 0.1% was applied along with the pure oil. It is observed that the temperature rises lentamente in nano-modified oil and reaches lower maximum temperature indicating the improvement in thermal property

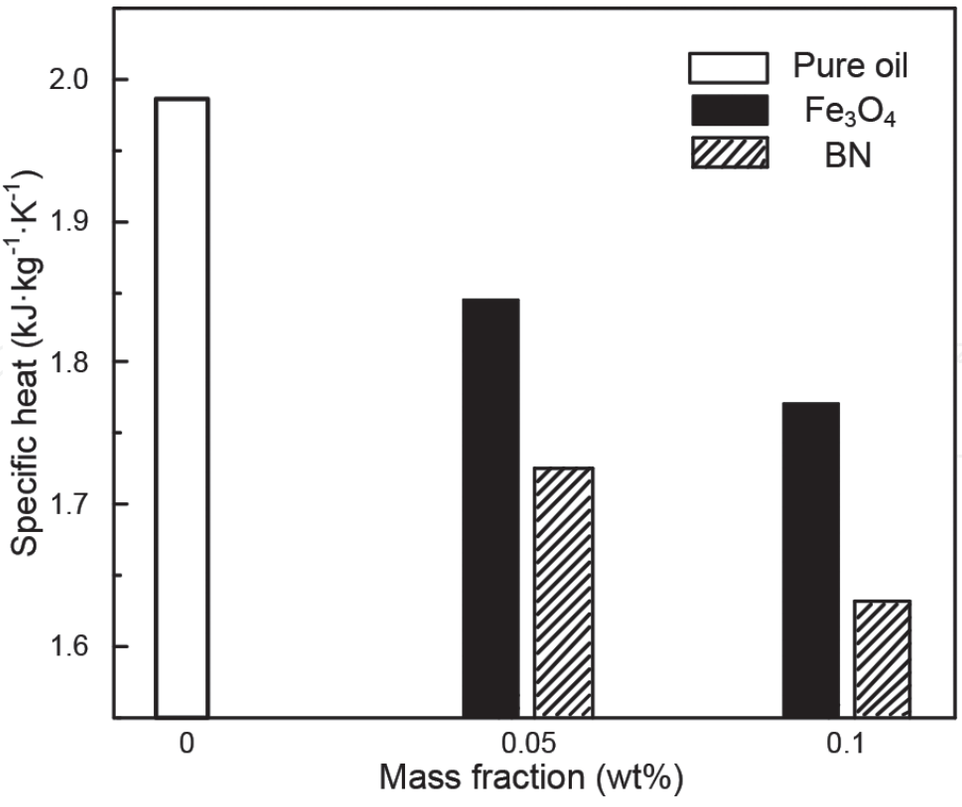

Figure 3. Relation between the specific heat and the mass fraction.

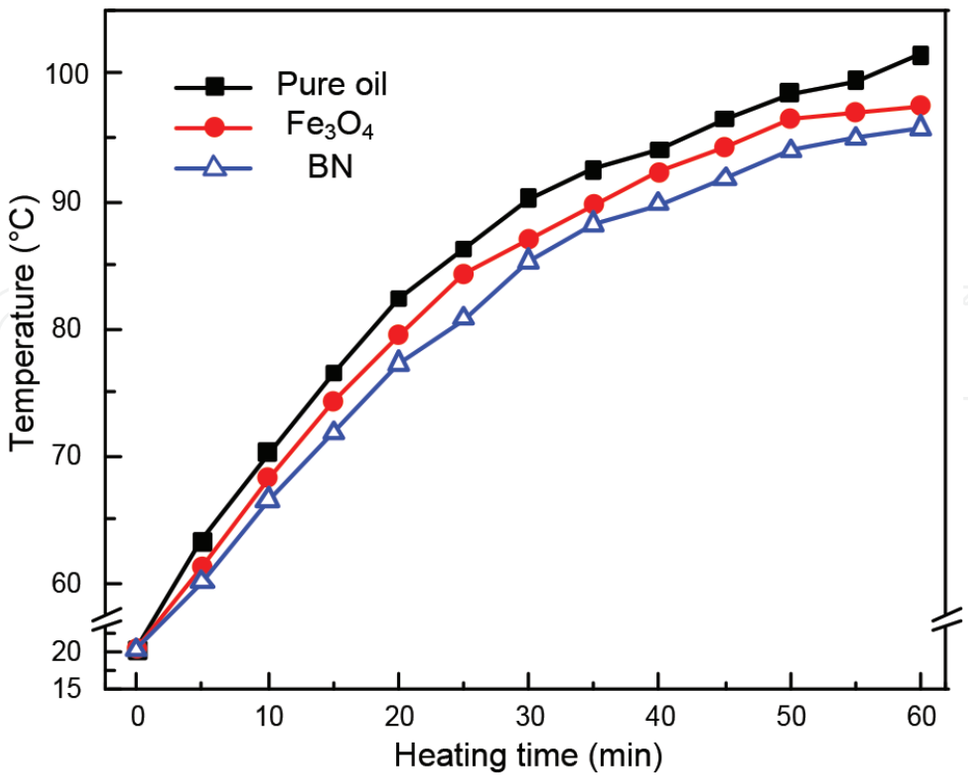

Figure 4. Relation between the heating coil surface temperature and the heating time with the different transformer oil.

with the addition of nanoparticles. For the two types of the nanooil, the temperature of the Fe_3O_4-modified nanooil shows faster increasing tendency compared with the BN-modified nanooil.

Since the nanooil was confirmed to have higher thermal conductivity and thermal diffusivity in previous tests, the heat generated by the coil is expected to be conducted and dissipate to the entire oil in a faster way due to the addition of nanoparticles especially for the BN-modified nanooil. The applied thermal tests confirm the fact that due to the excellent property in thermal conductivity, the transformer oil modified by BN nanoparticles performs superior thermal property compared to the Fe_3O_4-modified oil.

2.3. Effect on dielectric properties

The relative permittivity of the samples is shown in **Figure 5** as a function of the temperature. The oil dispersed with Fe_3O_4 nanoparticles shows higher value than the BN-modified oil at the same temperature and mass fraction. For all the prepared oil samples, the pure oil obtains the lowest value in relative permittivity at the same experimental condition, while the BN-modified oil at the mass fraction of 0.1% achieves nearly the same value as the Fe_3O_4-modified oil at a lower mass fraction of 0.05 wt% in the temperature range. Since the relatively permittivity of transformer oil is lower than the oil-impregnated pressboard, the increase is considered to be beneficial in causing a more uniform electrical field in oil-paper insulation system. As can be seen, the variation of relative permittivity to temperature change for the pure oil performs the same decline tendency as the nano-modified oil.

http://dx.doi.org/10.5772/67432

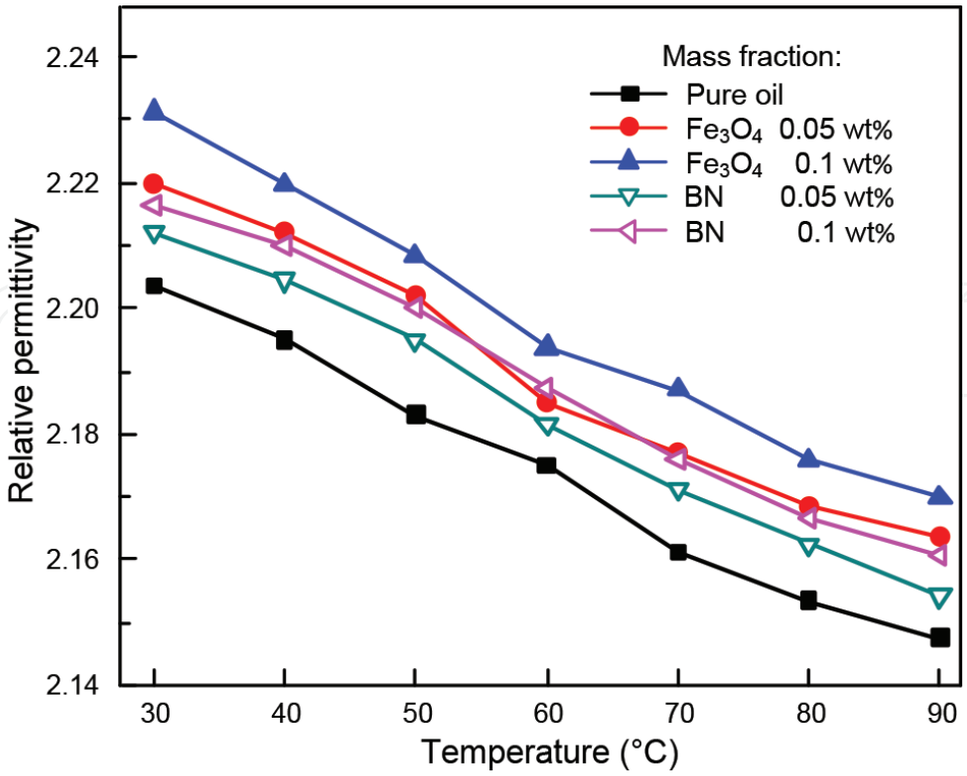

Figure 5. Relation between the relative permittivity and the temperature with the different mass fractions.

The increase of thermal agitation due to temperature rise would make it more difficult for the dipoles to orient and cause the slight decrease in relative permittivity consequently [9]. Due to the high relative permittivity of the additional nanoparticles, the nanooil shows enhanced dielectric property in relative permittivity. Thereby, the higher relative permittivity of Fe_3O_4 nanoparticles causes the higher relative permittivity of the Fe_3O_4-modified nanooil compared to the oil with BN nanoparticles.

Figure 6 shows the measured dissipation factor of the oil at the mass fractions of 0, 0.05 and 0.1% in the temperature range from 30 to 90°C. It is noticed that the dissipation factor of the Fe_3O_4-modified oil is larger than the nonmodified oil and increases with increasing the mass fraction, while the BN-modified oil shows lower value to the pure oil indicating the improved dielectric property with the addition of BN nanoparticles. As can be seen, the dissipation factor of all the oil samples shows the similar tendency in the temperature range. Furthermore, with increasing the mass fraction, the increasing tendency slows down obviously for the BN-modified oil.

The change of dissipation factor to temperature variation is considered to be mainly due to the change of electrical conductivity at constant frequency. Electrical conductivity significantly increases with temperature as a result of both the increasing dissociation of oil molecule and the decreasing oil viscosity leading to the obvious increase in dissipation factor [10].

The electrical resistivity decreases with increasing the temperature and varies with different additional nanoparticles as shown in **Figure 7**. With increasing the temperature, the carrier mobility depending on viscosity increases resulting in the decrease of electrical resistivity

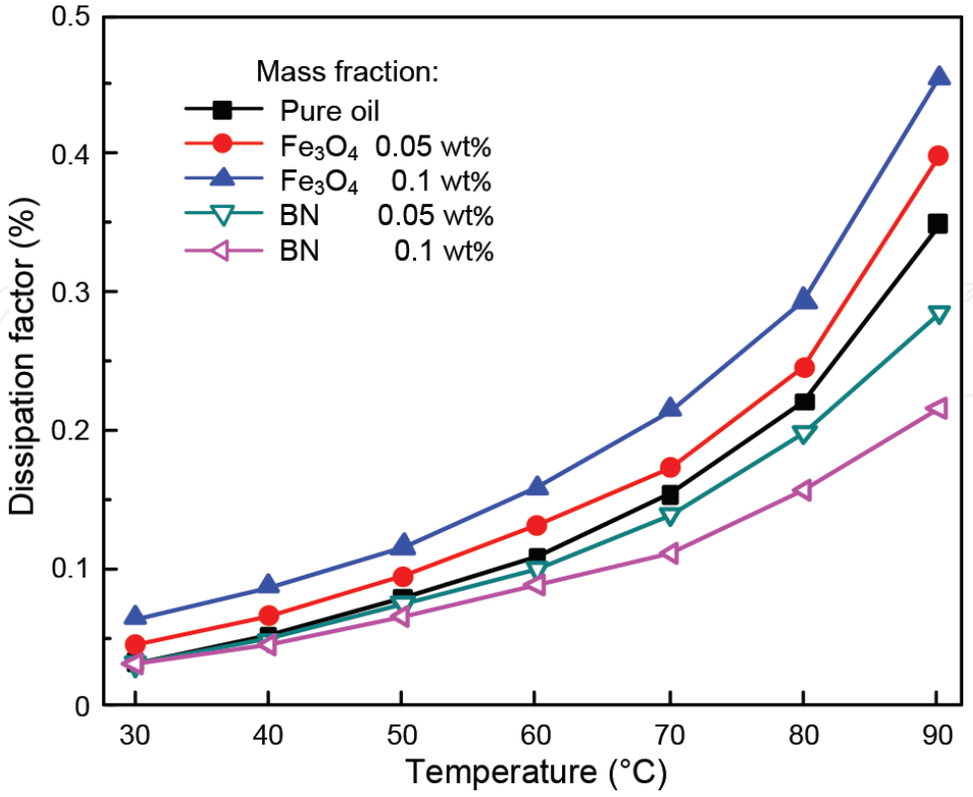

Figure 6. Relation between the dissipation factor and the temperature with the different mass fractions.

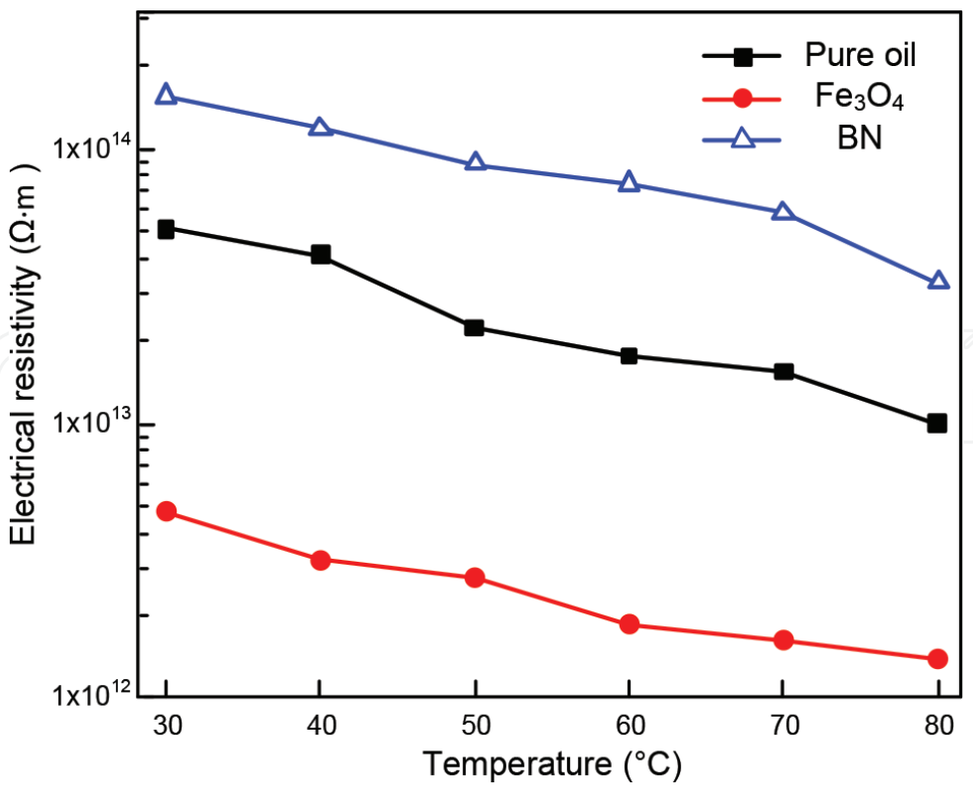

Figure 7. Relation between the electrical resistivity and the temperature with the different transformer oil.

http://dx.doi.org/10.5772/67432

as the characteristic of ionic conduction [11]. It is observed that the transformer oil modified with BN particles shows enhancement compared to the pure oil under the same temperature, while the Fe_3O_4-modified nanooil shows obvious lower value of electrical resistivity confirming the different behaviors between the two types of nanooil in dissipation factor as the result obtained above. The difference in resistivity is regarded as the consequence of the different electrical conductivity of the nanoparticles according to the model for nanooil [12].

2.4. Effect on breakdown strength

The ac breakdown strength varying with temperature and mass fraction is illustrated in **Figure 8**. The ac breakdown strength increases with increasing temperature and follows the similar tendency for all the oil samples. It is observed that the breakdown strength of the nanooil is higher than that of the pure oil in the range of temperature. Moreover, the Fe_3O_4-modified oil reaches even higher value than the BN-modified oil at the same condition. With the increase of mass fraction, the breakdown strength of nanooil rises obviously for both types of the nanooil. As shown in **Figure 9**, the dc breakdown strength of the specimens performs the similar tendency as the nanooil in ac breakdown strength test.

According to the multicore model by Tanaka, the nanoparticles create an interfacial region, which contributes to the improvement in the dielectric strength [13, 14]. It is considered that

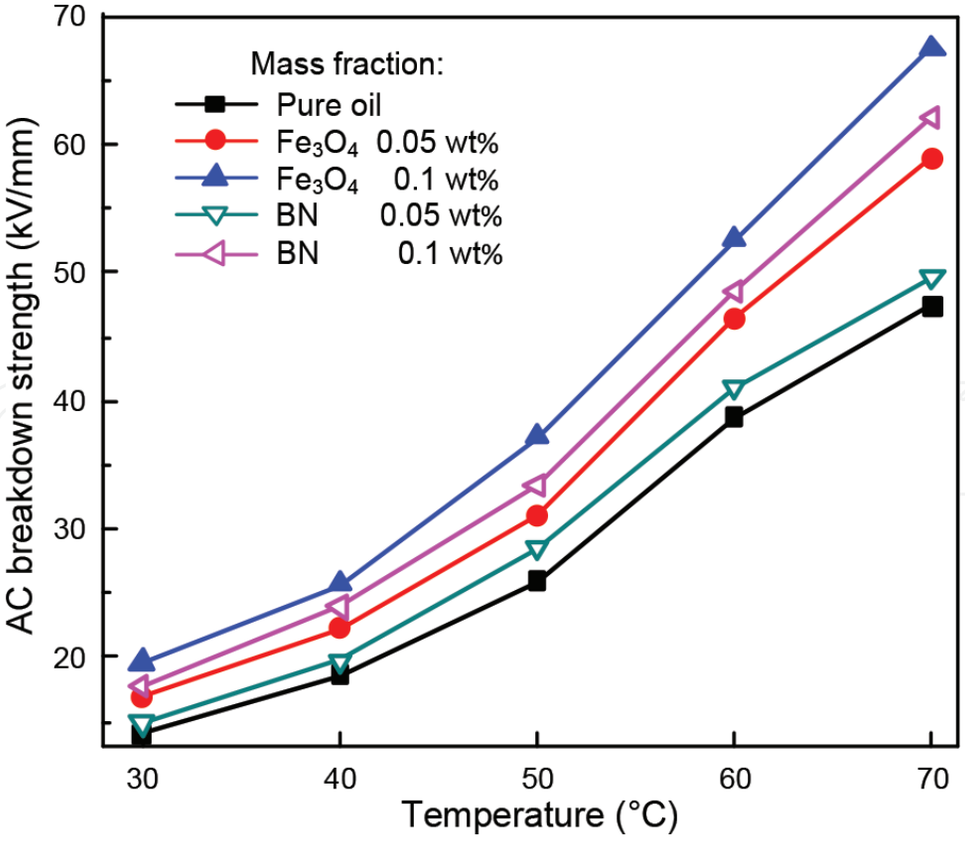

Figure 8. Relation between the ac breakdown strength and the temperature with the different mass fractions.

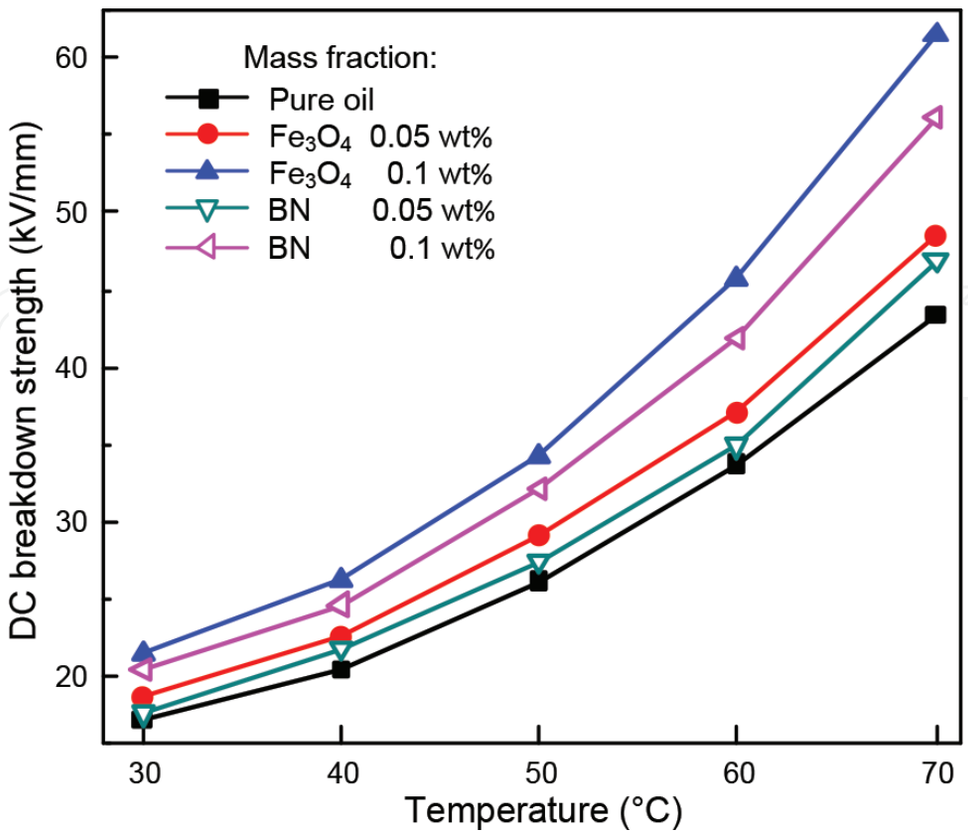

Figure 9. Relation between the dc breakdown strength and the temperature with the different mass fractions.

the percentage saturation dominates in the variation of breakdown strength during the range of temperature [15]. As temperature rises up, the absolute moisture content shows no obvious improvement, while the water solubility increases with temperature. Thereby, the breakdown strength shows the similar increasing tendency with the rise of temperature. Furthermore, Hwang et al found that the charge relaxation time constant can indicate the influence of nano-filter on the electrodynamic process in streamer propagation and explain the obvious enhancement in electric property of the nanooil [11]. Therefore, the different relaxation time constant of the nanoparticles can be explained for the different behaviors in breakdown strength.

Kao suggested a bubble theory for dielectric breakdown in liquid that the breakdown is initiated by bubbles which elongate and cause the formation of conducting channel in liquid gap and eventually result in the occurrence of breakdown due to electrons accelerating [16]. Furthermore, it is considered that the Joule heat generated at the electrodes due to the injection of carries may cause the initial formation of the bubbles [17]. It can be concluded that in the nanooil with enhanced thermal property, the faster heat dissipation to the vicinity results in the inhibition of bubble formation. As can be seen from **Figures 8** and **9**, the nanooil modified with BN nanoparticles shows more obvious improvement compared to the Fe_3O_4-modified oil when the mass fraction increases from 0.05 to 0.1% at the same temperature, which should attribute to the considerable enhancement in thermal property of the BN-modified oil when increase the mass fraction.

http://dx.doi.org/10.5772/67432

The difference in density due to temperature could lead to buoyancy-driven natural convection and cause heat dissipation. Moreover, the viscosity of the liquid shows increase when introduced with nanoparticles [17, 18] and hence may affect natural convection as reported [19]. The change in density and convection could lead to influence on fluid circulation and thus cause effect on the breakdown strength as the flow rate is considered as an important factor on breakdown behavior [15]. However, due to the slight filler loading, no significant increase of the viscosity is expected in the nanooil especially at high temperature. Thereby, it can be concluded that the influence of nanoparticles on convection and the consequent fluid circulation performs no obvious function on the dielectric breakdown strength [20]. Through the analysis and comparison above, it is expected that besides the effect of relaxation time constant, the improved thermal property functions as a considerable factor in the remarkable enhancement of the breakdown strength.

3. Dynamic behavior of surface charge on double-layer oil-paper insulation under pulse voltage

3.1. Experiments

In the research, the paper used in the experiment is produced by Nantong Zhongling Co. Ltd. The oil in the experiment was 25# and produced by Kunlun Energy. Insulation paper with the thickness of 0.13 mm was chosen and cut into the size of 70 mm × 50 mm. The oil and paper were dried at 373.15 K for 24 h first. Then, the paper was immersed into the oil and continued to be dried at the same temperature for another 12 h [22–24]. Finally, the oil-paper composite was placed in the vacuum oven.

3.2. Effect of voltage amplitudes

To show variation characteristics of the surface potential under different voltage amplitudes more clearly, the potential data from 0 to 1200 s are chosen in **Figure 10**, in the partly-enlarged graph, while the trend with the longer time from 0 to 30,000 s is shown in smaller graph. From the two figures, the potential decreases with the increase of time. The decay is fast at the initial period and then becomes slower with the time. The trapped charges in shallow traps are easy to escape, causing the rapid decay at the initial time. With increasing the time, the detrapping of charges in deep traps occurs, and thus, the decrease of surface potential slows down. The lateral charge spreads along the possible routes for charge decay. It either transports through the bulk or recombines with the opposite polar ions in air. The charge is initially transferred from the surface to the bulk in the electric field, then it is trapped and detrapped, and after these processes, the charge finally reaches the grounded electrode [21].

It is also observed in **Figure 10** that as the voltage amplitudes applied in this experiment are significantly different, the difference in initial surface potential is obvious in these curves. It is shown in **Figure 10a** that with different amplitudes, the decay trend is almost the same. However, the initial values of the potential are ~300, ~1550, ~1750 and ~2300. It can be concluded

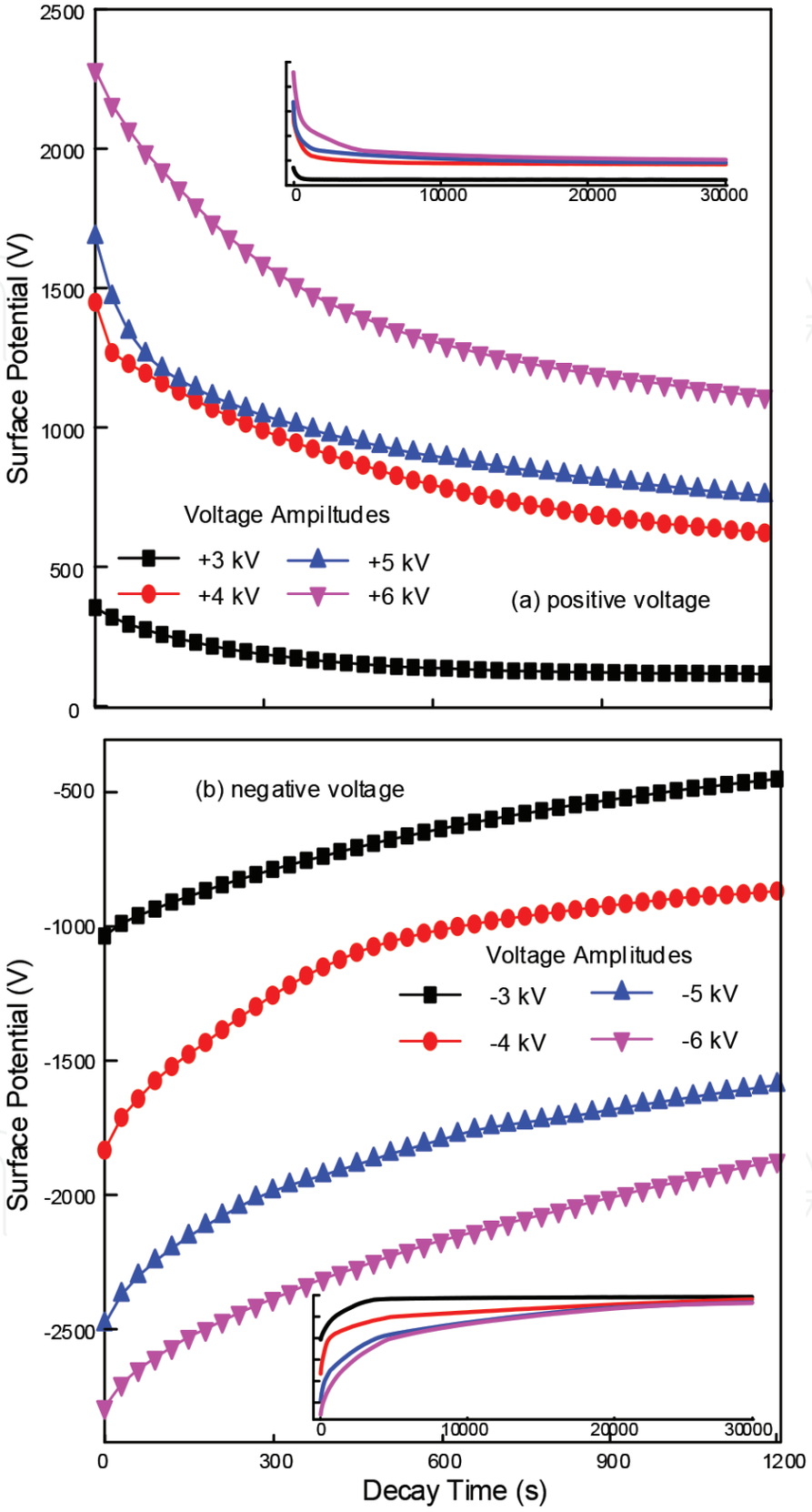

Figure 10. Relationship between the surface potential and the decay time, after a pulse voltage with a frequency of 500 Hz and pulse number of 12,000, with different voltage amplitudes and polarities.

http://dx.doi.org/10.5772/67432

that the increase of voltage amplitudes causes the increase of the surface potential, which indicates that more charge could be injected into paper under the higher pulse voltage [22]. With the time lapse, the surface potential of all four curves decreases. But due to the difference of initial potential value, the curves do not have crossover phenomenon. The surface potential under +3 kV voltage is much lower than that in other cases, which indicates that charge injection needs a threshold value. Only the voltage is applied over this value can the charge be injected into the hole. From **Figure 10b**, things are almost the same. Comparing with the positive pulse voltage, the absolute value of the initial surface potential under the negative pulse voltage is higher under the same experimental conditions. It means that the quantity of positive charges accumulated on the surface is less than negative charges, and it also infers that detrapping process of positive charge is easier than that of negative charge [23].

The relationship between the $t\mathrm{d}V/\mathrm{d}t$ and the decay time is shown in **Figure 11**. A double exponential decay equation has been used to analyze the decay curve of surface potential, and it was assumed that there were two kinds of decay process [24]. For the $t\mathrm{d}V/\mathrm{d}t$ curves in **Figure 11a**, it can be inferred that the first peak with a smaller characteristic time corresponds to a faster decay process that the charges escape from the shallow trap, while the second peak with a larger characteristic time is related to a slower decay process that the charges run away from the deep trap. It is clearly showed that the amplitudes of the maximum peak value of +3, +4, +5, and +6 kV are ~80, ~350, ~420, and ~470. Also the corresponding characteristic time changes from 300 to 8000 s, expressing that the peak value and the characteristic time increase in the order of +3<+4<+5<+6 kV. However, in **Figure 11b**, things are different. For the negative pulse voltage, all the four curves have only one peak, indicating that there is only one changing peak of the charge in the corresponding trap depth. When the negative voltage is applied in the paper, a compound peak occurs in the curve.

Furthermore, the negative charge is hard to escape from the traps because it is captured by oil-paper more easily. While the peak values of the curves with the voltage amplitudes of −3, −4, −5 and −6 kV are ~300, ~370, ~700 and ~900, respectively. It is the same with **Figure 11a**, which indicates that with increasing the voltage amplitudes, the peak value of the curves grows. But the characteristic time increases in the order −4<−3<−6<−5 kV. The results show that the duration of the charge decay process with different samples is effected by the voltage amplitudes, but the negative voltage plays a leading role in the characteristic time.

3.3. Effect of pulse frequency

In order to realize how the pulse frequency affects the oil-paper insulation, the relationship between the initial value of surface potential and the pulse frequency is shown in **Figure 12**. Actually, the surface potential of all samples declines quickly in the initial decay period, and then it decreases a little slower than that in the initial time. Moreover, from **Figure 12a**, the initial surface potential in 500, 750 and 1000 Hz with the pulse number of 12,000 is 1565, 1520 and 1324, respectively, which indicates that the initial value of the three curves is very close, while with pulse frequency increasing, the initial becomes a little bit smaller. It indicated that the frequency will slightly affect charge accumulation. **Figure 12b** also corresponds to the same rules, but the absolute value of the surface potential is a bit larger than that in **Figure 12a**.

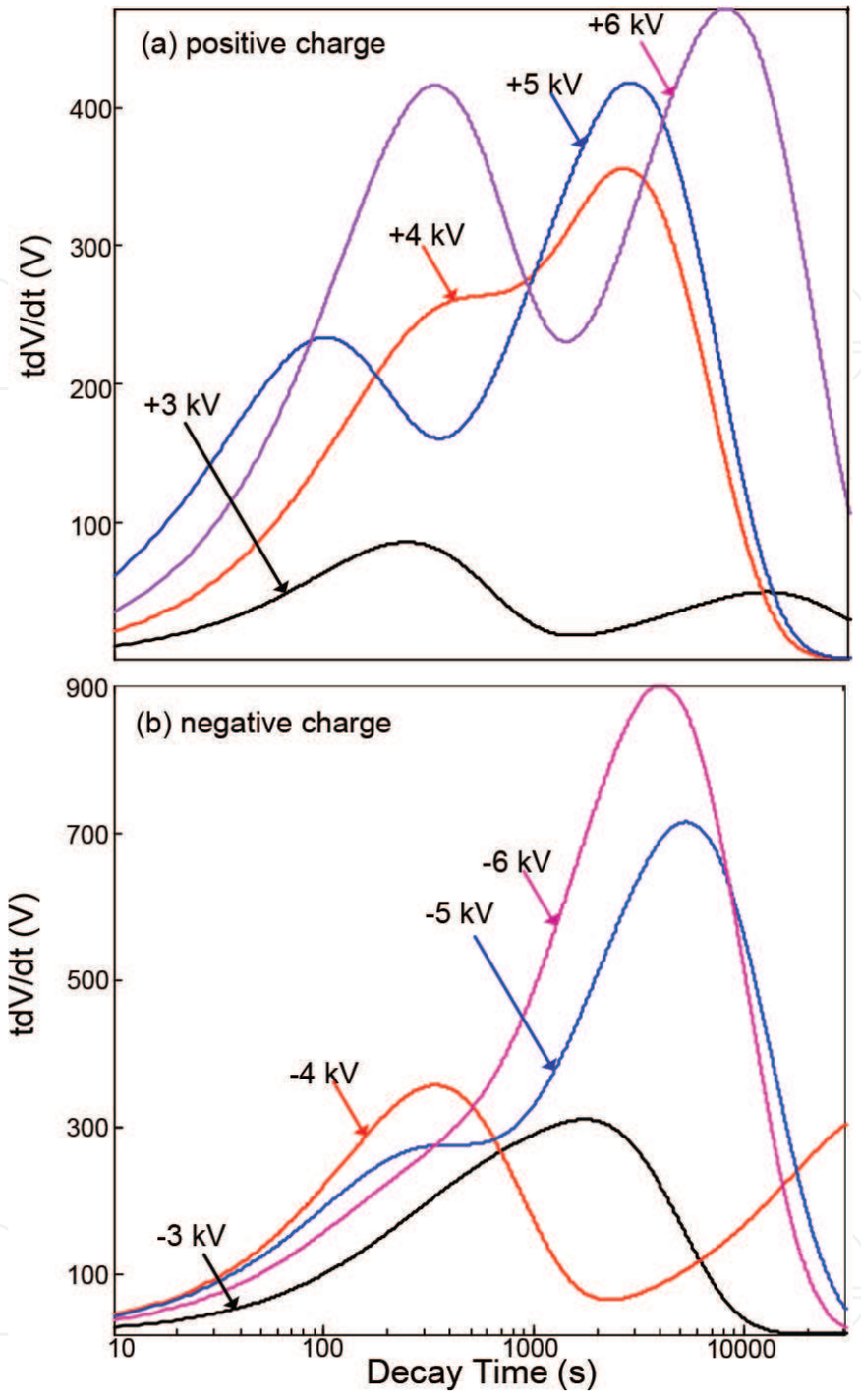

Figure 11. Relationship between the *t*d*V*/d*t* and the decay time, after a pulse voltage with a frequency of 500 Hz and pulse number of 12,000, with different voltage amplitudes.

The relationship between the decay rate and the pulse frequency is shown in **Figure 13**. From **Figure 13a**, with the frequency of 500, 750 and 1000 Hz and the pulse number of 12000, the decay rates are 38.2, 44.6 and 52.2%, indicating that with the increase of pulse frequency, the decay rate grows. When the frequency is high, the charge does not have enough time to enter the shallow traps and the energy of injecting charges per unit time becomes higher, then the surface charge becomes less and declines faster. And during the process of charge injection,

http://dx.doi.org/10.5772/67432

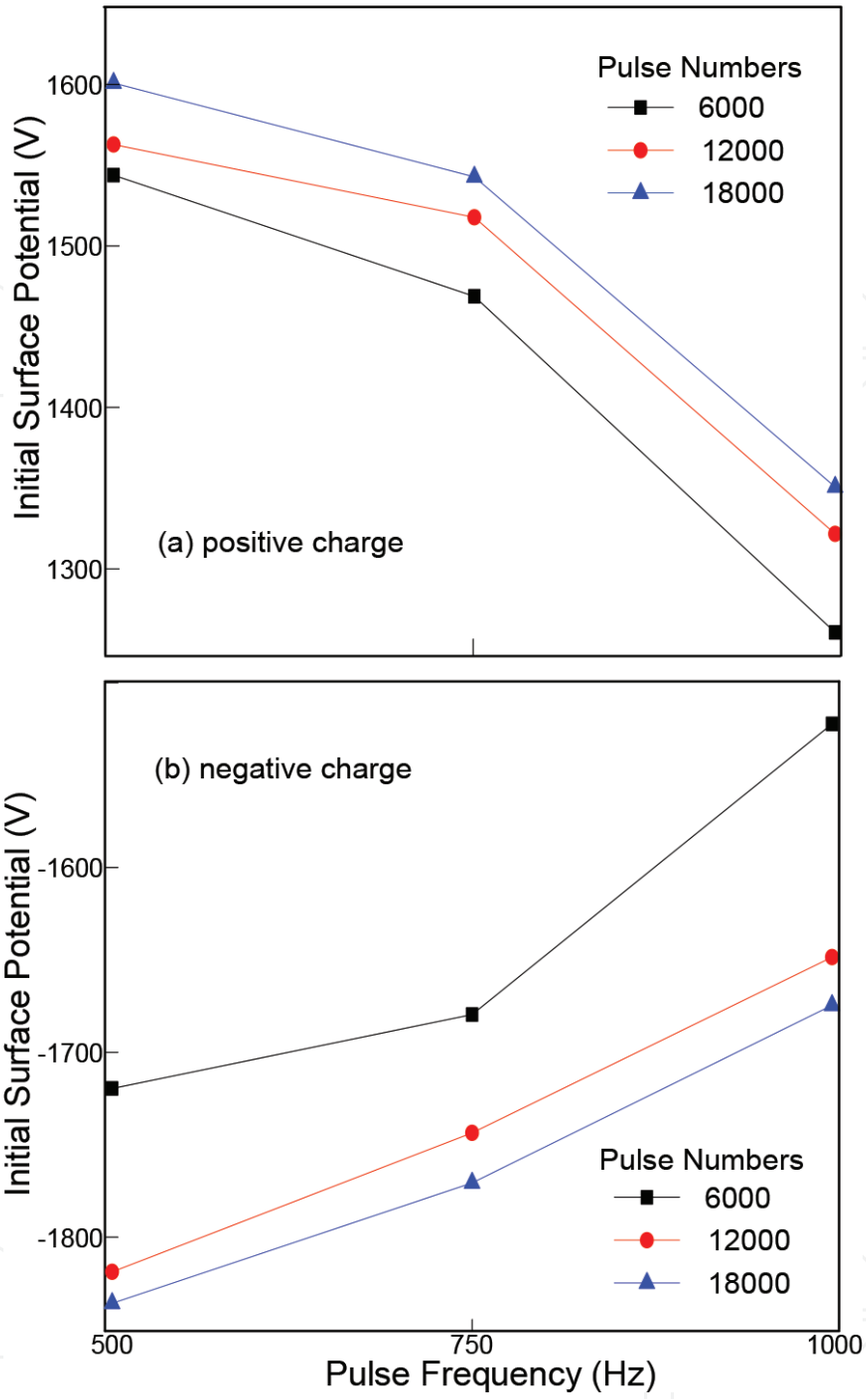

Figure 12. Relationship between the initial surface potential and the pulse frequency, after a pulse voltage with a voltage amplitude of ±4 kV, with different pulse numbers.

the charge injected previously dissipates more because of the higher energy. The decay rate under the negative charging in **Figure 13b** is smaller than that of the positive one, which is due to the detrapping process of negative charge is more difficult than that of positive charge.

Figure 14 displays the relationship between the $t\mathrm{d}V/\mathrm{d}t$ and the decay time, under different pulse frequency. As in **Figure 14a**, most of the curves also have two peaks for the positive voltage. It is obvious that the maximum peak values of 500, 750 and 1000 Hz are ~290, ~230 and

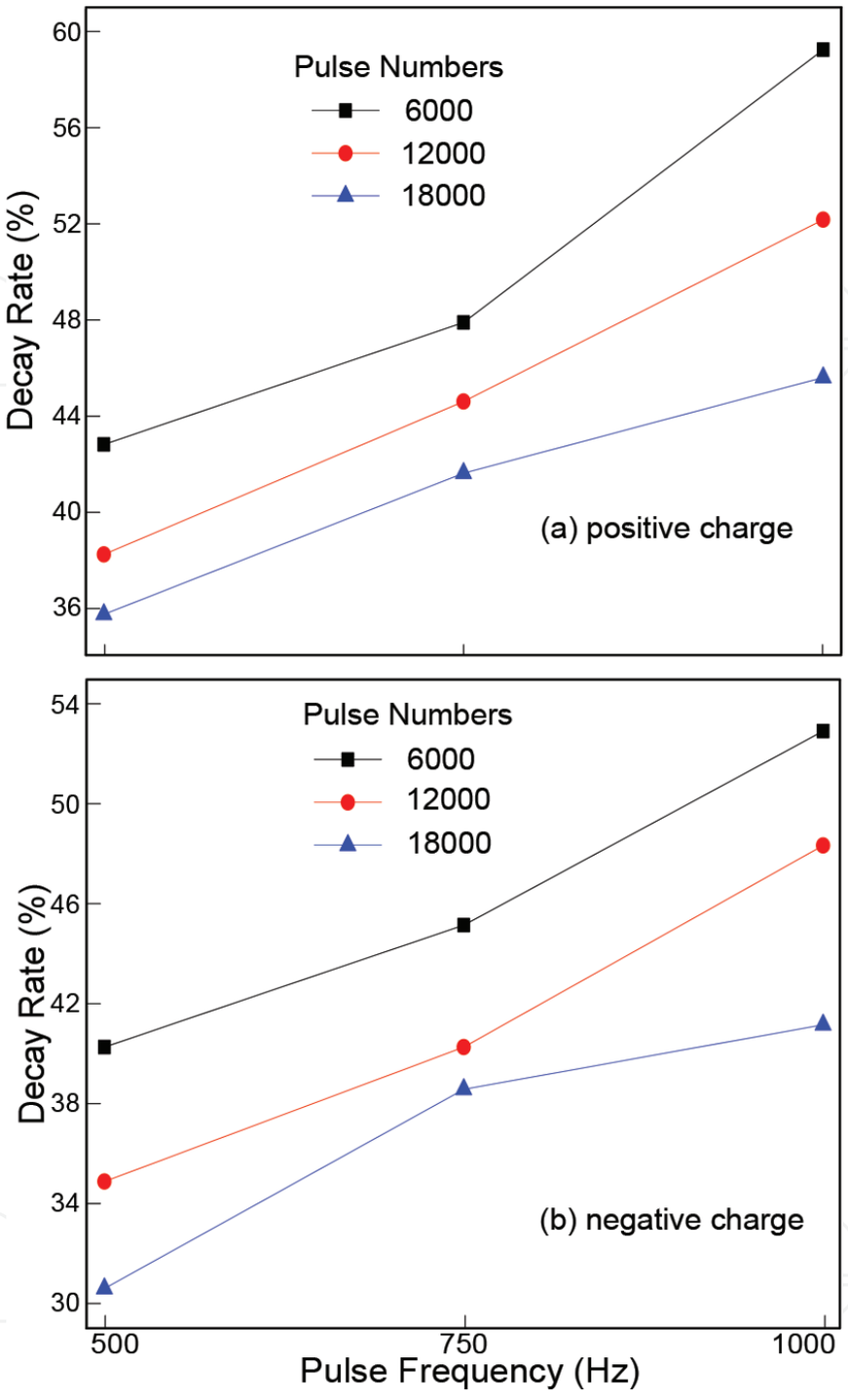

Figure 13. Relationship between the decay rate and the pulse frequency, after a pulse voltage with a voltage amplitude of ±4 kV, with different pulse numbers.

~190, respectively, indicating that the peak value decreases as the frequency grows. The first characteristic time changes from 100 to 1000 s, showing that the decay time decreases with the increase of pulse frequency. In this case, for the sample under the pulse voltage of 1000 Hz, the peak value is the smallest and the characteristic time is the shortest. So the phenomenon in **Figure 15a** accords with that in **Figure 13a**. The similarity is in the case with the negative

http://dx.doi.org/10.5772/67432

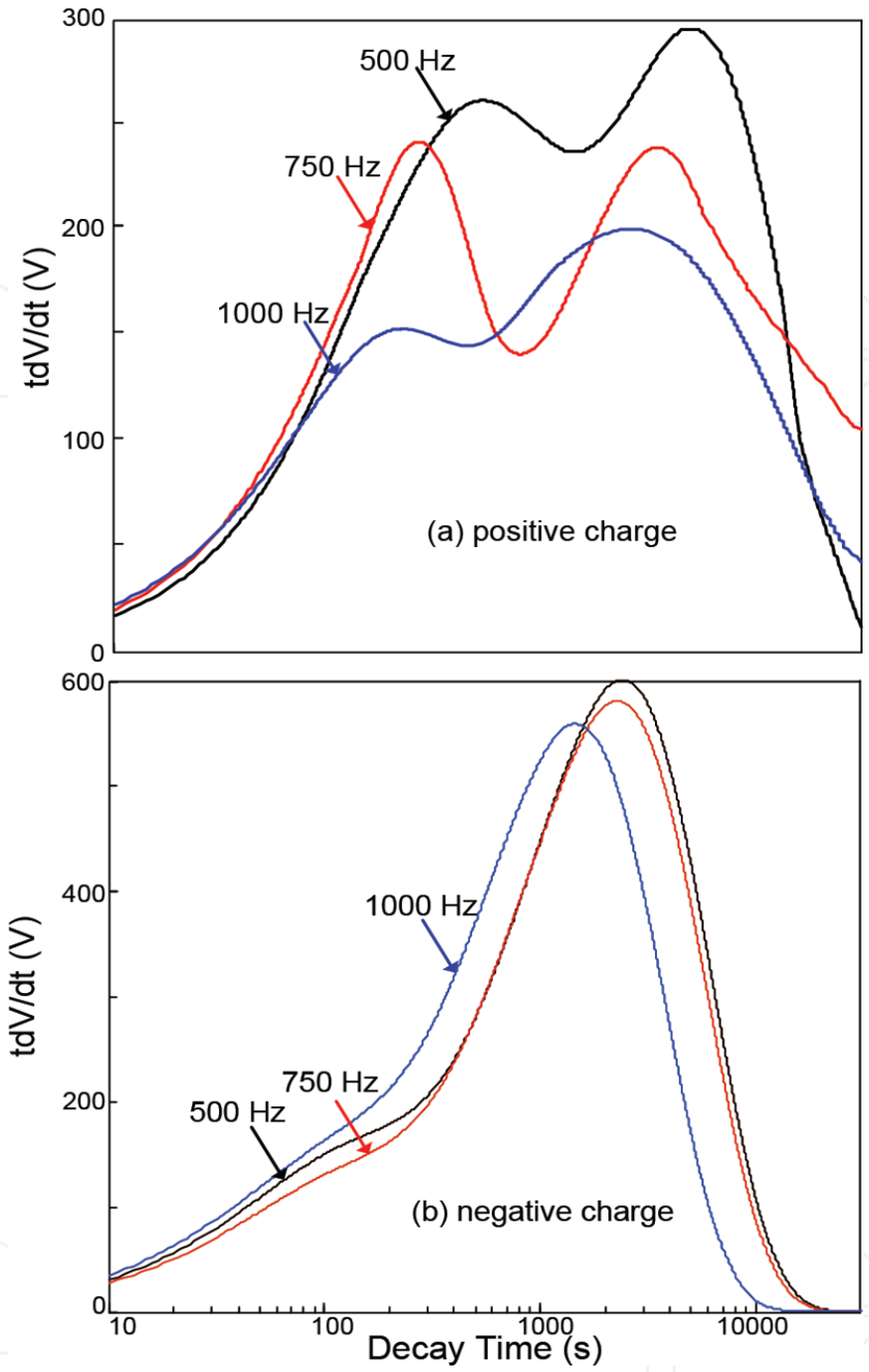

Figure 14. Relationship between the *t*d*V*/d*t* and the decay time, after a pulse voltage with a voltage amplitude of ±4 kV and pulse number of 12,000, with different pulse frequencies.

voltage in **Figure 14b**. For the negative voltage, there is only one peak in every three curves, indicating that there is only one changing peak of the charge in the corresponding trap depth. Also, the peak values of the curves with the frequency of 500, 750 and 1000 Hz are ~600, ~580 and ~550, respectively, which reveals that the increase of the frequency causes the *t*d*V*/d*t* to decrease. The characteristic times decrease with the growth of frequency. It is similar to the situation in **Figure 14a**.

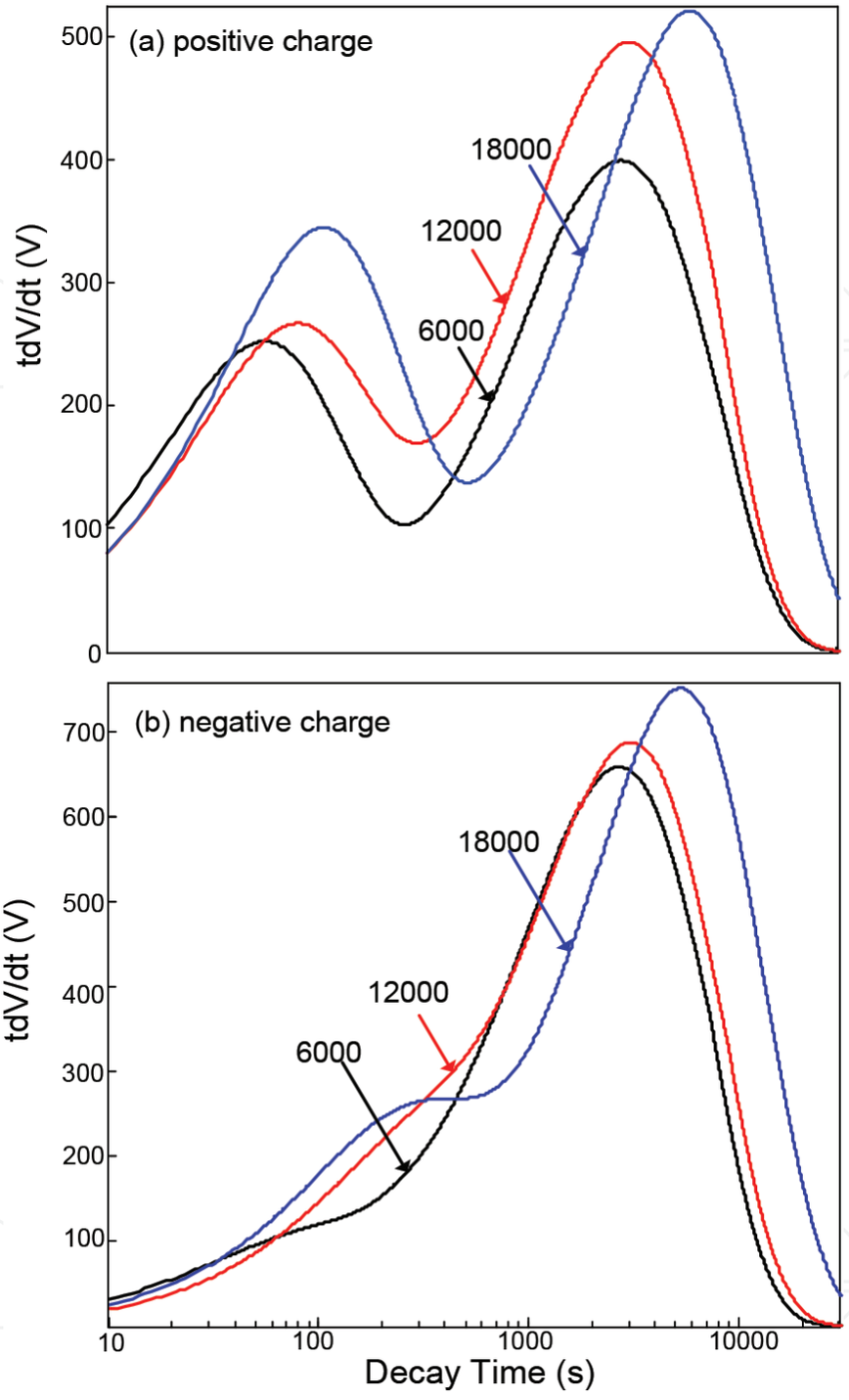

Figure 15. Relationship between the *t*d*V*/d*t* and the decay time, after a pulse voltage with a voltage amplitude of ±5 kV and pulse frequency of 750 Hz, with different pulse numbers.

3.4. Effect of pulse numbers

Figure 12 also reflects the relationship between the initial surface potential and the pulse numbers under ±4 kV pulse voltage. It is shown in **Figure 12a** that the initial surface potentials under the pulse numbers of 6000, 12,000 and 18,000 with the frequency of 750 Hz are 1471, 1520 and 1545, respectively, showing that with the increase of pulse numbers, the initial

http://dx.doi.org/10.5772/67432

value gets bigger. Actually, when the pulse voltage is applied to the electrode, some ions that are produced by the previous pulse would still exist until the next one comes, which is called the accumulation effect [11]. Therefore, more charges would be easily injected into the surface under more pulses. Also, with increasing pulse numbers, more charges tend to accumulate in the deep traps. **Figure 13a** shows the relationship between the decay rate and the pulse numbers. The decay rate with the pulse numbers of 6000, 12,000 and 18,000 under 750 Hz is 47.9, 44.6 and 41.6%, which expresses that increasing pulse numbers results in a slower charge dissipation. Due to more charges pumped into the deep traps, they would escape from the deep traps and return back to the surface of the paper. So the dissipation of the charges under more pulse numbers would be slowly. **Figures 12b** and **13b** show the similar trend that the absolute value of the potential under the negative pulse voltage is bigger than that under the positive one, while the decay rate is smaller, indicating that the negative charge accumulates more and dissipates more slowly.

Figure 15 shows the relationship between the $t\mathrm{d}V/\mathrm{d}t$ and the decay time, under different pulse numbers. For the positive voltage, as in **Figure 15a**, most of the curves also have two peaks. And the maximum peak often appears on the second peak. It is obvious that the maximum peak values of 6000, 12,000 and 18,000 pulse numbers are ~400, ~480 and ~530, respectively, which expresses that the peak value increases with the pulse number growing. The first characteristic time changes from 30 to 100 s, indicating that the decay time increases with the growth of pulse numbers. Actually, the second characteristic time also corresponds to the same rule. The peak value is the highest, and the characteristic time is the longest for the paper under the pulse number of 18,000. From **Figure 15b**, the negative voltage is in the similar situation. For the negative voltage, there is only one peak in each curve, indicating that there is only one changing peak of the charge in the corresponding trap depth. Also, the peak values of the curves with the pulse numbers of 6000, 12,000 and 18,000 are ~650, ~680 and ~750, respectively, which reveals that the growth of the pulse number causes the $t\mathrm{d}V/\mathrm{d}t$ to increase. The characteristic time changes from 2000 to 4000 s, and it increases as the numbers grow.

4. Charge coupling behavior of double-layer oil-paper insulation under DC and pulse voltages

4.1. Experiments

In this research, insulation paper with a thickness of 0.13 mm was chosen and cut to the size of 70 mm × 50 mm. Then, the transformer paper was dried at 373.15 K for 24 h. Later, the paper was immersed in the oil and continued to be dried at the same temperature for another 12 h. Finally, the composite oil-paper was laid into the vacuum oven for 1 day.

4.2. Effect on charge coupling with different voltage waveforms

Figures 16 and **17** show the relationship between the surface potential and the decay time. **Figure 16a** shows the situation where the oil-paper insulation was applied to positive DC and pulse voltages. As the pulse voltage amplitudes applied in this experiment are different, initial

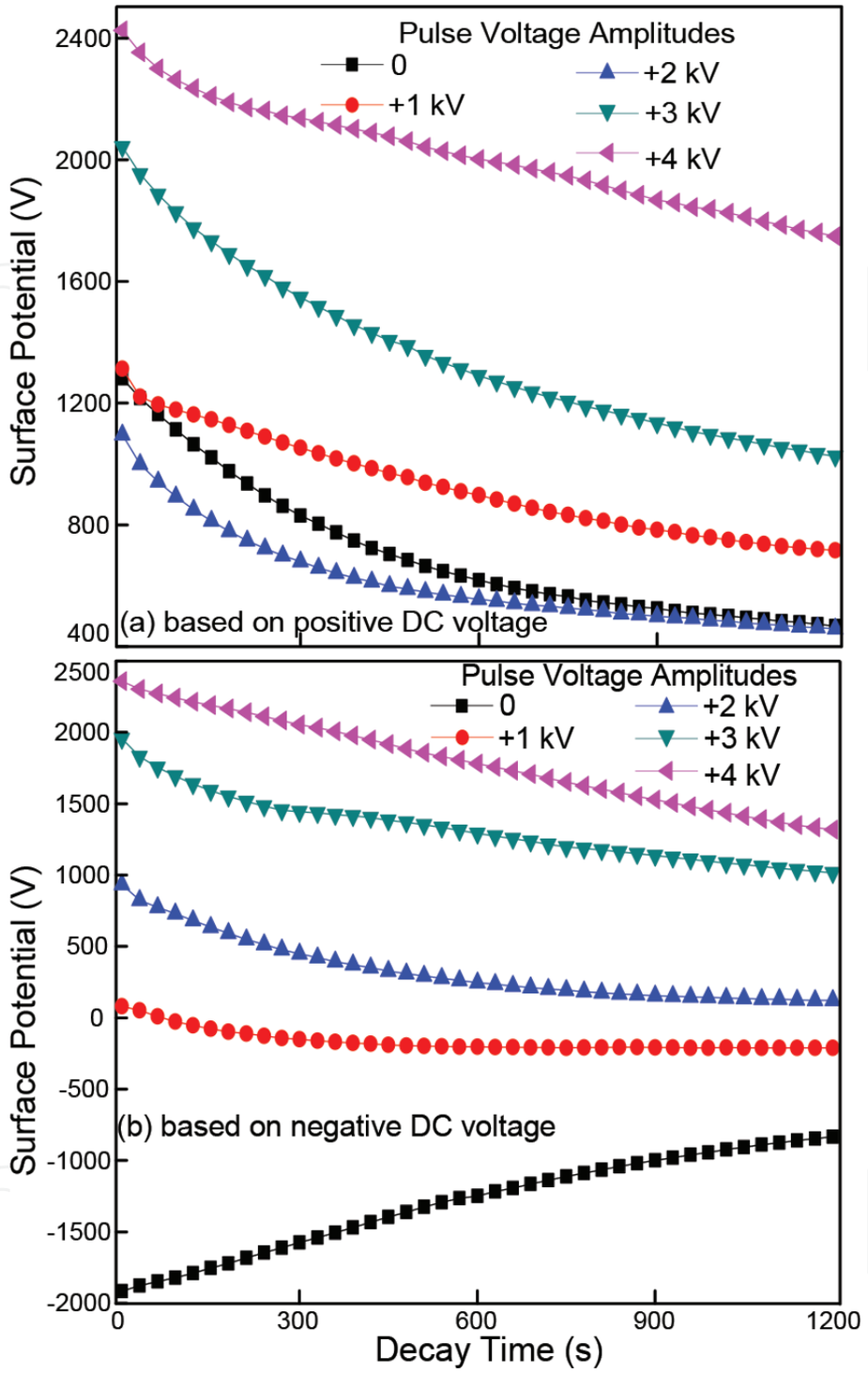

Figure 16. Relationship between the surface potential and the decay time, after an application of DC and positive pulse voltage with a frequency of 500 Hz and pulse numbers of 6000, with different voltage amplitudes.

values of the surface potential are obviously different in these curves. **Figures 16b** and **17a** show that, with the increase of pulse voltage amplitudes, the charge with the same polarity as the pulse voltage increases. It is not the same as the situation in **Figures 16a** and **17b** when compared with the initial values. **Figure 18** represents the rules more obviously. According to

http://dx.doi.org/10.5772/67432

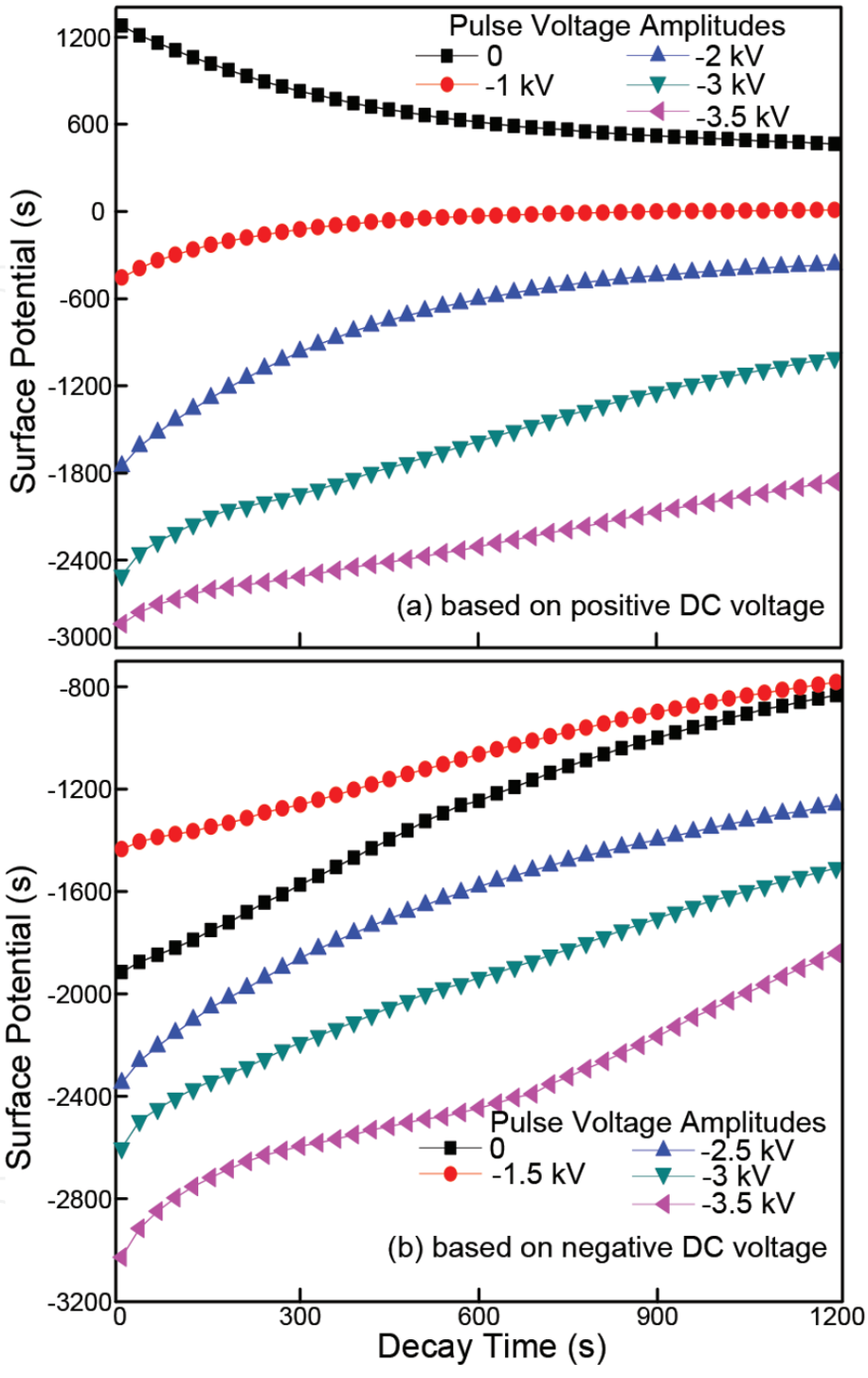

Figure 17. Relationship between the surface potential and the decay time, after an application of DC and negative pulse voltage with frequency of 500 Hz and pulse numbers of 6000, with different voltage amplitudes.

the two figures, when the DC and pulse voltages are in the same polarity, the curves show a clear inflection point. When the polarity becomes the opposite, the curves show a single trend.

Now, taking **Figure 18a** as an example, when the pulse voltage amplitudes are changing from 0 to 1 kV, the initial surface potential maintains a fixed value. As the amplitude gets larger,

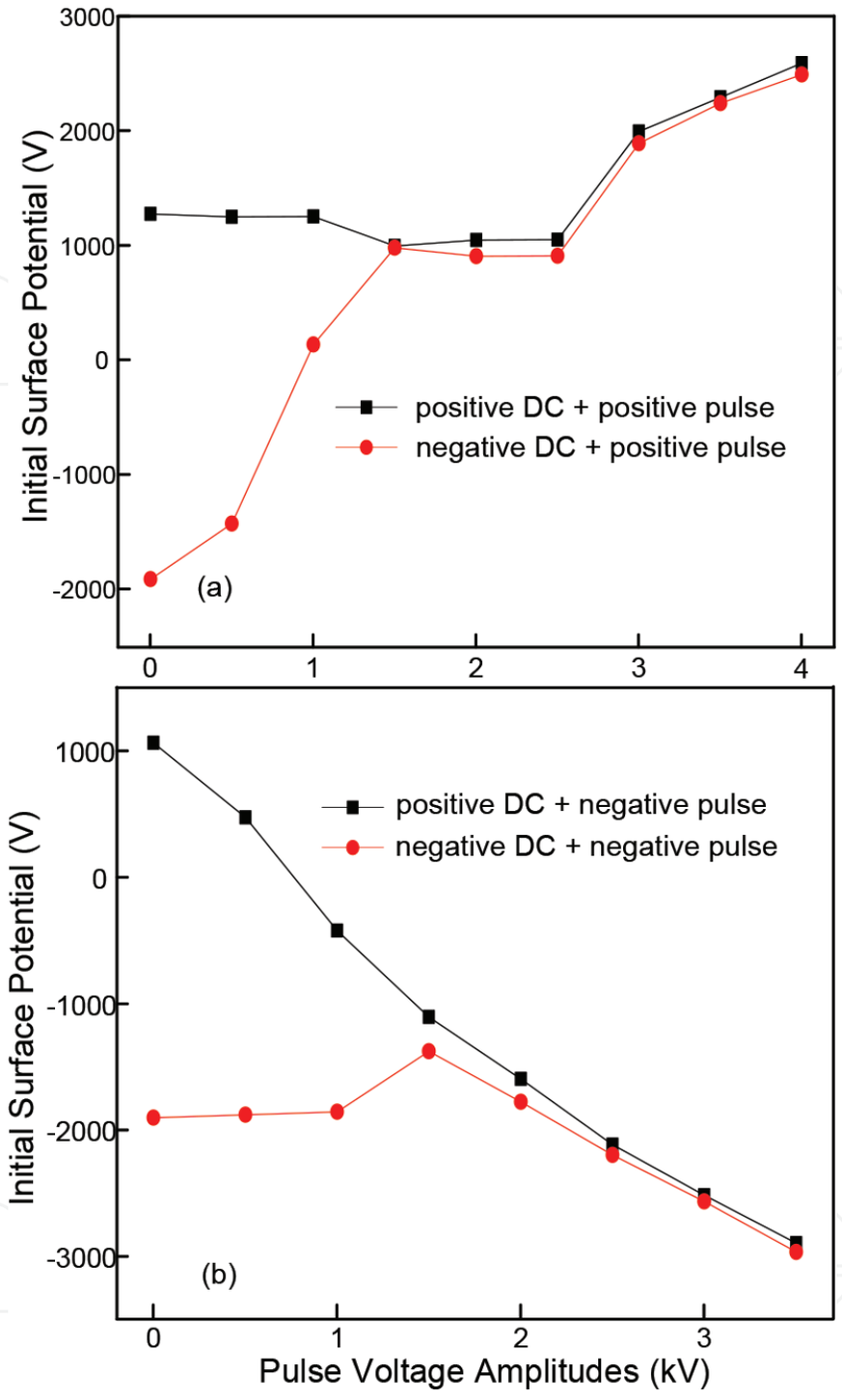

Figure 18. Relationship between the initial surface potential and the pulse voltage amplitudes, after an application of DC and pulse voltage with frequency of 500 Hz and pulse numbers of 6000.

the initial value decreases instead. Furthermore, as the amplitude continues to increase, the initial value grows. In this case, the illustration of charge coupling and accumulation is shown in **Figure 19**. As the DC voltage is applied to the sample, large number of charge are injected from the needle to the sample. Under the same amplitude and duration of DC voltage, the amounts of surface charge are certain. When the pulse voltage amplitude is small enough,

http://dx.doi.org/10.5772/67432

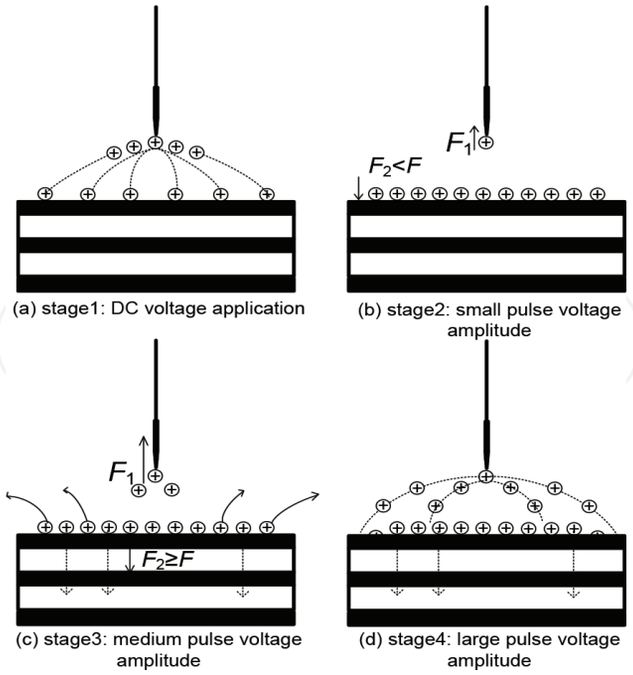

Figure 19. Illustration of surface charge coupling and accumulation, after an application of +3 kV DC and positive pulse voltages in different amplitudes.

which means that the amplitude is no more than 1 kV, as in **Figure 19b**, a small quantity of charge will be injected from the needle.

According to Coulomb's law, due to the repulsive force of the homo-charge, the charge from the needle will no longer be injected into the sample, and of course, the repulsive force F_2 is too small to make the charge from the surface transport through the bulk or recombine with the opposite polar ions in the air ($F_2<F$). So, small pulse voltage amplitude has little effect on initial surface potential. When the amplitude ranges from 1.5 to 2.5 kV, as in **Figure 19c**, the charge from the needle increases with the rise of the amplitude. So, the repulsive force F_1 and F_2 increases. Although the charge from the needle cannot reach the surface of the sample under the repulsive force, some charge from the oil-paper interface will be acted on by enough force to transport through the bulk or neutralize with the opposite polar ions in the air ($F_2 \geq F$). So, the surface charge and the initial surface potential reduce. With the pulse voltage amplitudes increase continuously, as in **Figure 19d**, for more than 2.5 kV, the charge from the needle continues to increase more. At that time, as a result of the strong force and the strong energy of the applied electric field, the pulse voltage will "push" the charge from the needle to the surface of the paper, thus easily raising the surface charge density. So the initial value of the potential will definitely increase, and more charge will be accumulated on the surface of the paper.

When it comes to the negative DC and pulse voltages, the trend is almost the same. The only distinction is that, when the voltages are both positive, as in **Figure 18a**, there will be an almost horizontal line, indicating that when the amplitude of pulse voltage is between 1.5 and 2.5 kV, the initial value of surface potential is almost the same; on the contrary, when the voltages are both negative, as in **Figure 18b**, there is only the highest surface potential, which means that the surface charge is the least at the 1.5 kV pulse voltage. Actually, a positive

charge is relatively hard to accumulate on the sample, so homocharge interaction in positive polarity has a relatively complex and long transient process, leading to the lowest saturation values. On the other hand, during the interaction of the negative homo-charge, it is easy to accumulate negative charge.

The illustration of charge coupling and accumulation after a negative DC voltage and a positive pulse voltage applied is shown in **Figure 20**. In the initial stage, due to the negative DC voltage, the negative charge accumulates on the surface of the sample. Then, the positive pulse voltage is applied, and when the voltage amplitude is small, according to **Figure 20b**, on account of Coulomb's law, only small numbers of positive charge are applied to the surface and neutralize with the negative charges. So, there is still some negative surface charge remaining. With the increase of pulse voltage amplitude, more positive charge is pushed to the surface and recombines with the negative. When +1 kV pulse voltage is applied to the sample, from **Figure 20c**, the quantities of positive and negative charge are basically equal. So, the initial surface potential is almost zero. From **Figure 20d**, it can be seen that, as the pulse voltage continues to increase, more positive charge will accumulate on the surface, so the value of the surface potential tends to become positive. When it comes to a positive DC and a negative pulse voltage, the trend is almost the same as that with a negative DC voltage and a positive pulse voltage applied. The only difference is that, when the pulse voltage is positive, as in **Figure 18a**, there will be an almost horizontal line, meaning that when the pulse voltage amplitude is between 1.5 and 2.5 kV, the initial surface potential is almost the same, while when the pulse voltage is negative, as in **Figure 18b**, with the pulse voltage amplitudes increasing, the initial surface potential declines.

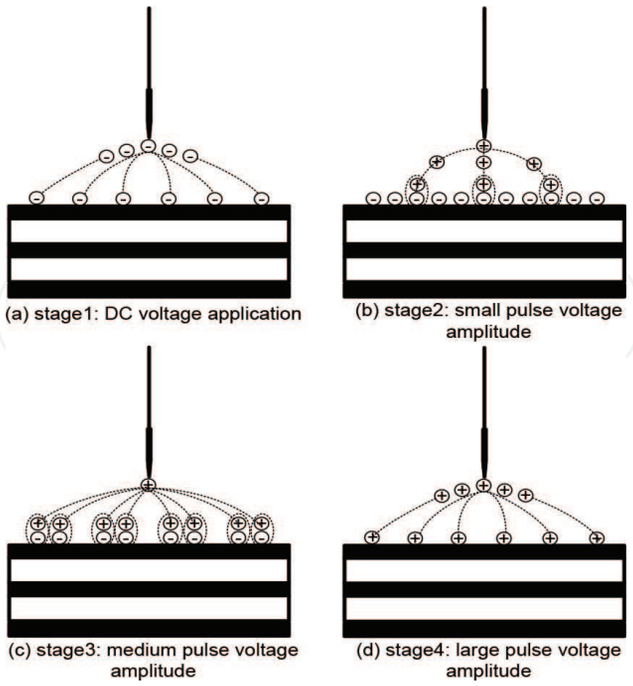

Figure 20. Illustration of surface charge coupling and accumulation, after an application of −3 kV DC and positive pulse voltages in different amplitudes.

Furthermore, from **Figure 18**, it is obvious that, for the same pulse voltage, the absolute initial value of the DC voltage in the same polarity is higher than that in a different polarity, especially for the pulse voltage over 1 kV. Actually, in this situation, with the increase in the amplitude, the gap between the two curves is reduced, but always exists. The reason for this phenomenon is that as DC voltage is in different polarity, the charge polarity is different as well. As the pulse voltage is applied to the sample, it plays a major role in charge accumulation. So the gap decreases with the increase in amplitude. Even so, the charge in the same polarity will increase on the surface, while that in different polarity will first recombine, and then the charge in the same polarity with the pulse voltage will be accumulated. So the absolute value of the DC voltage in the same polarity is ultimately higher than that in different polarity.

Comparing **Figure 18a** and b, the absolute value of the initial surface potential under the negative pulse voltage is larger than that under the positive pulse voltage for a pulse voltage over 1.5 kV. This shows that less positive charge than negative charge is accumulated on the surface, which infers that the detrapping process of the negative charge is more difficult than that of the positive charge [25].

Truly, the pulse voltage surely makes a greater difference than the DC voltage. Through experimental studies, it is obvious that a few pulse voltages over a short time play an important role in charge accumulation. In other words, pulse voltage amplitude indeed greatly affects surface charge. So, pulse voltage is a destructive voltage. Lightning and operating impulse voltages are both factors that may trigger the breakdown of oil-paper insulation. So, it is necessary to ascertain the mechanism of charge coupling and accumulation after DC and pulse voltages, especially the effect of pulse amplitudes.

4.3. Effect on charge coupling with different pulse numbers

In order to understand the effect of pulse numbers on oil-paper insulation, the relationship between the initial surface potential and the pulse numbers is expressed in **Figure 21**. From **Figure 21a**, the initial surface potentials with the pulse numbers of 10, 50, 100, 500, 1000, 3000, 6000, 12,000 and 18,000 for positive DC and pulse voltages are 1872, 1983, 2050, 2112, 2287, 2304, 2342, 2387 and 2390, respectively. Meanwhile, the initial surface potentials with those pulse numbers for a negative DC voltage and a positive pulse voltage are 1787, 1831, 1975, 2083, 2178, 2205, 2242, 2275 and 2346, respectively. The two curves reveal that the initial value of these data shows evident gaps, but the resemblance is that with the increase in pulse numbers, the initial values become a little larger. Meanwhile, as the voltage continues to rise, the initial value increases slowly and becomes gradually saturated. Actually, when the pulse voltage is applied to the electrode, some ions produced by the previous pulse still exist until the arrival of next pulse, and this is called the accumulation effect [26]. Therefore, under more pulses, more charge would be easily injected into the surface, and when the pulse voltage is high enough, there is enough charge accumulated on the surface. Due to the repulsive force, the remaining charge from the needle can no longer be injected to the sample and thus recombines with the opposite polar ions in the air. So the initial value rises with the increase in the pulse number and then comes to saturation. In **Figure 21b**, the two curves show a similar trend, revealing that regardless of the polarities of the DC and pulse voltages, the increase of

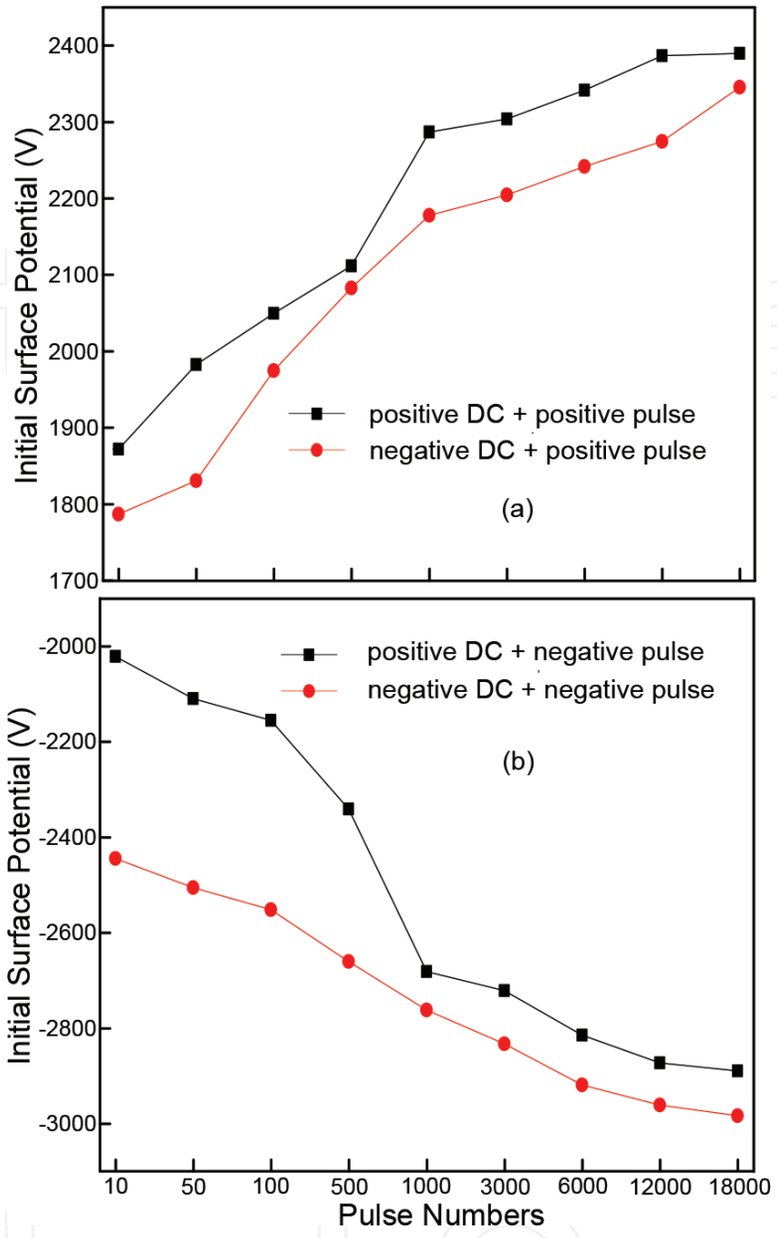

Figure 21. Relationship between the initial surface potential and the pulse numbers, after an application of DC and pulse voltage with voltage amplitude of 3.5 kV, with different voltage polarity.

the pulse number will cause more surface charge to be accumulated, and at last to be saturated. Also, it is evident from these two figures that, when the DC and pulse voltages are in the same polarity, more charge will be accumulated.

The relationship between the decay rate and the pulse number is shown in **Figure 22**, with different voltage polarity. For positive DC and pulse voltages, the decay rates with the pulse numbers of 10, 50, 100, 500, 1000, 3000, 6000, 12,000 and 18,000 are 50.4, 47.4, 44.1, 42.0, 39.0, 36.1, 34.2, 31.1 and 28.7, respectively. Also, for a negative DC voltage and a positive pulse voltage, the decay rates with the corresponding pulse numbers are 57.7, 50.9, 49.7, 45.6, 43.2, 41.5, 37.5, 35.1 and 29.9, respectively. Actually, the other two curves show the same trend, which indicates that with the increase in pulse number, the decay rate decreases, and thus,

http://dx.doi.org/10.5772/67432

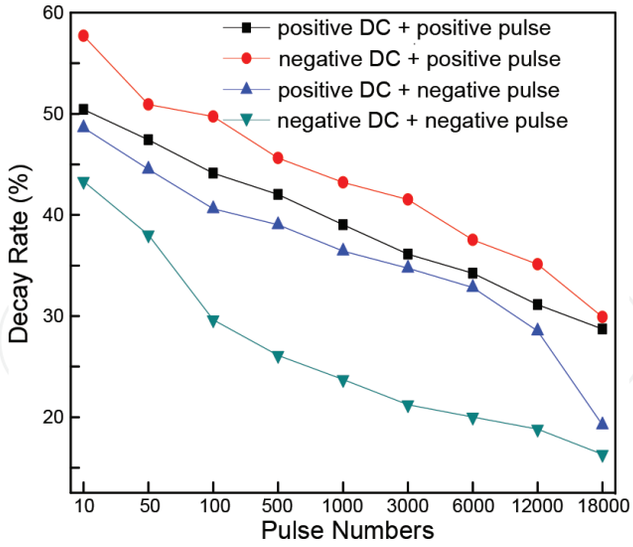

Figure 22. Relationship between the decay rate and the pulse numbers, after an application of DC and pulse voltage with voltage amplitude of 3.5 kV and pulse frequency of 500 Hz, with different voltage polarity.

the charge is dissipated slowly. This phenomenon is due to more charges being pumped into the deep traps, and they will escape from the traps and go back to the surface of the paper. So, the dissipation process of charges under higher pulse numbers would be slow. Also, for the same pulse numbers such as 500, it is easily summarized from the curves that the decay rates of positive DC and pulse voltages, a negative DC voltage and a positive pulse voltage, a positive DC voltage and a negative pulse voltage, and negative DC and pulse voltages are 42.0, 45.6, 39.0 and 26.1%, respectively. Other groups of data show the same trend, revealing that the decay rate decreases with the order as follows: a negative DC voltage and a positive pulse voltage, a positive DC and a positive pulse voltage, a positive DC voltage and a negative pulse voltage, and a negative DC and a negative pulse voltage. There are two reasons for this phenomenon. The main reason is that negative charges are easily accumulated in paper. So, when the negative pulse voltage was applied, the negative charge is easily accumulated and hard to get rid of the traps in the paper. The second reason is that hetero-charges will first recombine with each other, resulting in smaller amounts of surface charge. So, the DC and pulse voltage decay rates in the same polarity are lower than that in different polarity.

The relationship between the $t\mathrm{d}V/\mathrm{d}t$ and the decay time is shown in **Figure 23**, after a DC voltage and a positive pulse voltage were applied, with different polarity. In these figures, the characteristic time is defined as the time when the curves get to the peak value. For positive DC and pulse voltages, from **Figure 23a**, most of the curves have two peaks, and the maximum peak is usually the second peak. It is obvious that for the first peak values of 10, 50, 100, 500 and 1000, pulses are ~10,000, ~11,000, ~12,000, ~13,000 and ~25,000, respectively, indicating that the peak value increases as the pulse number grows. The first characteristic time changes from 200 to 2000 s, which shows that the decay time increases with the increase in pulse number. In this case, for the sample under the 1000 pulse voltage, the peak value is the largest and the characteristic time is the longest, while for the curve of 1000 pulses, a compound peak appears, showing that there is only one changing peak in the charge in the corresponding trap depth. The existence of the compound peak may be in line with the model

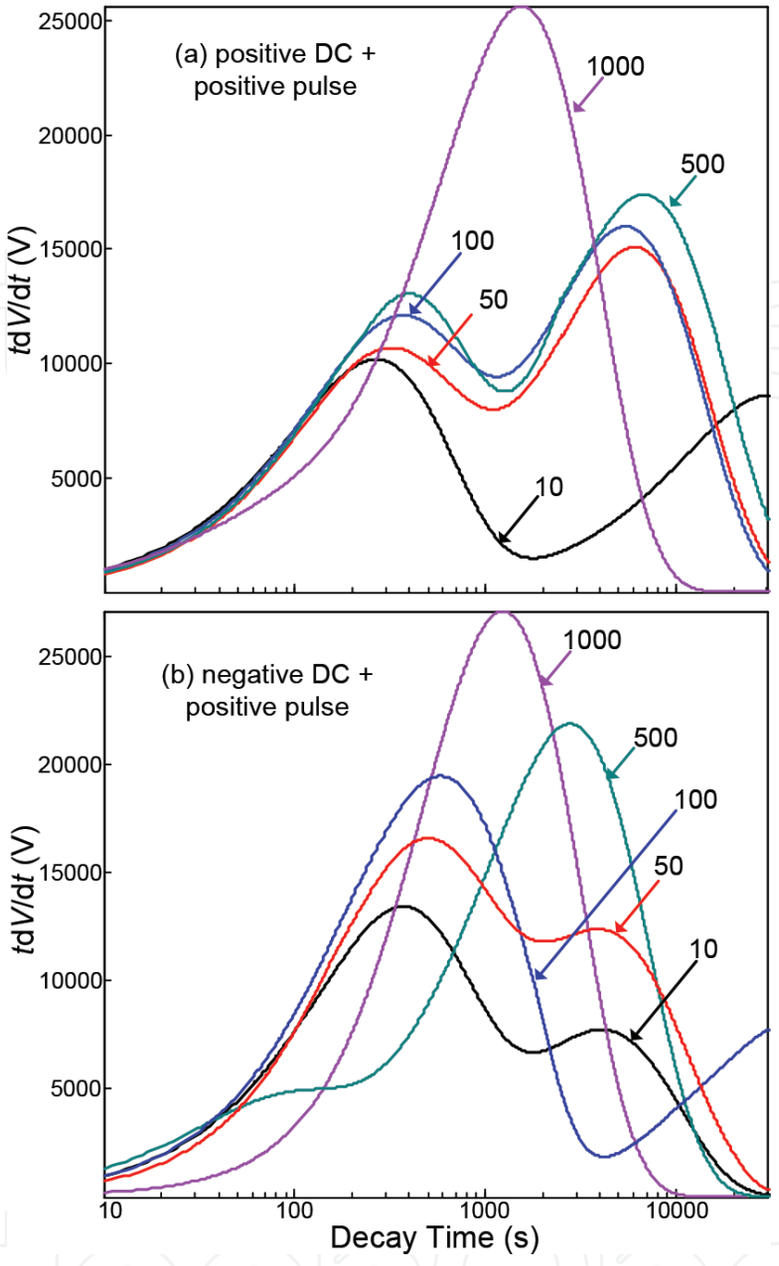

Figure 23. Relationship between the $t\mathrm{d}V/\mathrm{d}t$ and the decay time, after an application of DC and positive pulse voltage with the amplitude of 3.5 kV and pulse frequency of 500 Hz, with different voltage polarity.

proposed by Simmons, which considers the emission current from the closely spaced trapping level [27]. For **Figure 23b**, the initial peak values of the curves with pulses 10, 50, 100, 500 and 1000 are ~13,000, ~17,000, ~20,000, ~22,000 and ~27,000, respectively, also revealing that the growth in the pulse numbers causes the elevation in the $t\mathrm{d}V/\mathrm{d}t$. The first characteristic time changes from 300 to 3000 s, and it increases in the order 10<50<100<1000<500.

Figure 24 shows the relationship between the $t\mathrm{d}V/\mathrm{d}t$ and the decay time under a DC voltage and a negative pulse voltage. It is clear from **Figure 24a** that, all the five curves only have one peak and for the peak values of 10, 50, 100, 500 and 1000, the pulses are ~17,000, ~24,000, ~26,000, ~30,000 and ~36,000, respectively, indicating that the peak value increases with the

http://dx.doi.org/10.5772/67432

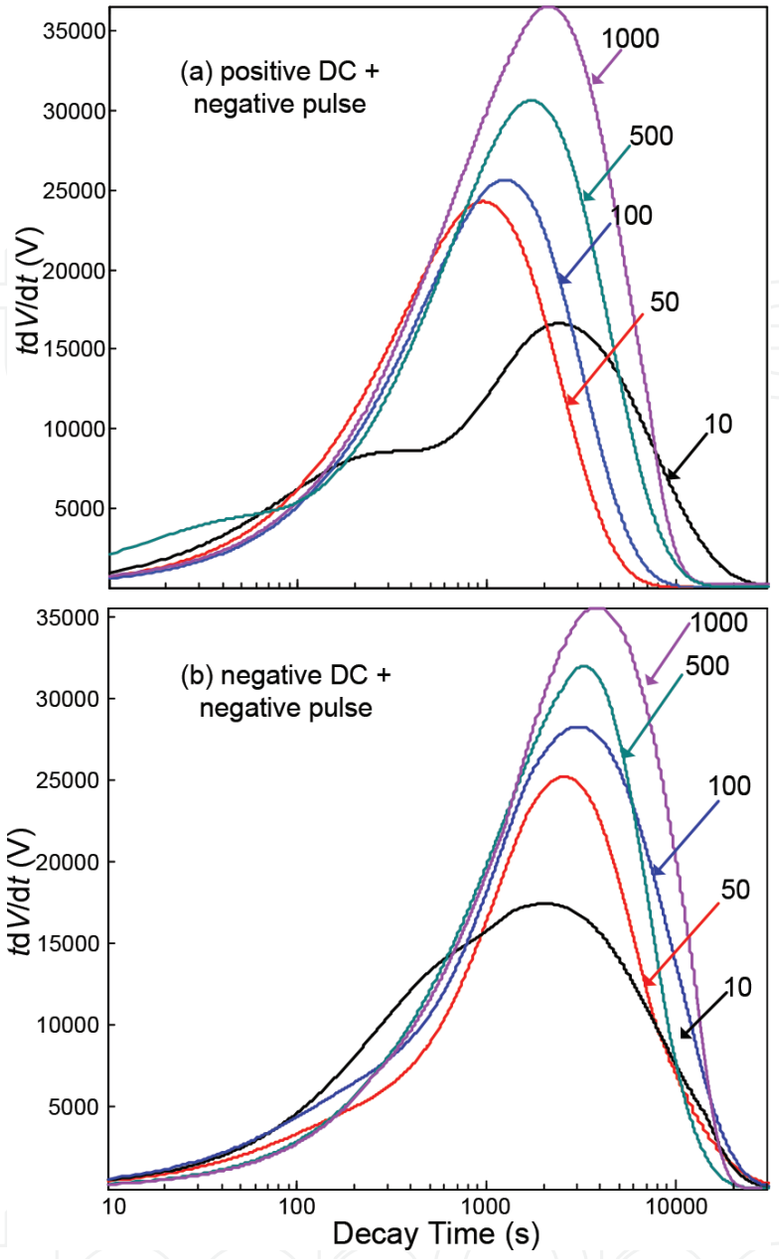

Figure 24. Relationship between the *t*d*V*/d*t* and the decay time, after an application of DC and negative pulse voltage with voltage amplitude of 3.5 kV and pulse frequency of 500 Hz, with different voltage polarity.

pulse number growing. The characteristic time changes from 800 to 2000 s, and it increases in the order 50<100<500<1000<10. From **Figure 24b**, for the negative DC and pulse voltages, there is only one peak in each curve, indicating that there is only one changing peak in the charge in the corresponding trap depth. Also, the peak values of the curves with the corresponding pulse numbers are ~17,000, ~25,000, ~28,000, ~32,000 and ~35,000, respectively, revealing that the growth in the frequency causes the rise in the *t*d*V*/d*t*. The characteristic time changes from 2000 to 4000 s, and it increases as the numbers enlarge. Also, in comparing **Figures 23** with **24**, it is obvious that the peak value of the negative pulse voltage is commonly larger than that of the positive pulse voltage, which probably means that the negative pulse voltage has higher corona discharge energy [28].

5. Conclusion

The effect of BN and Fe_3O_4 nanoparticles on thermal and dielectric characteristics of the transformer oil and the effect of voltage amplitudes, pulse frequencies, numbers and polarities were investigated. This chapter suggested a method to modify the properties of transformer oil, and obtained results illustrate obvious enhancement both in breakdown strength and in thermal properties due to the addition of nanoparticles. From the discussion of the relationship between the surface charge behavior and these key elements, there is better understanding of recognizing the charge coupling dynamics according to the surface potential and the $t\mathrm{d}V/\mathrm{d}t$ change rule between the paper layers in a multilayer insulation system. The main conclusions can be summarized as follows:

1. The thermal conductivity and thermal diffusivity increase with increasing the mass fraction of the two types of nanooil. The improvement could attribute to the interfacial region due to the additional nanoparticles and the ballistic phonon transport among the nanoparticles. The BN-modified nanooil shows superior thermal property in comparison with Fe_3O_4-modified oil due to the high thermal conductivity of BN nanoparticles.

2. Compared with the pure oil, the relative permittivity of the two types of nanooil is higher in the temperature range due to the high relative permittivity of the nanoparticles. The dissipation factor is lower, and electrical resistivity is higher in BN-modified oil while showing the opposite tendency in the Fe_3O_4-modified oil due to the different dielectric property of the two types of nanoparticles.

3. The breakdown strength of the two types of nanooil shows obvious enhancement with the addition of the nanoparticles which could attribute to the interfacial region created by the nanoparticles and increases with increasing the temperature due to the decrease of relative moisture content. The different improvement to mass fraction for the two types of nanooil indicates that the improved thermal property acts as an important role in the enhancement of breakdown strength according to the bubble theory.

4. With increasing the voltage amplitude, if the polarity of the DC and pulse voltages is same, the absolute value of the initial surface potential decreases initially and then increases, while, if two kinds of voltages are in different polarity, the charge with the same polarity as the pulse voltage increases. Furthermore, for the same pulse voltage, the absolute initial value of the DC voltage in the same polarity is higher than that in different polarity, and the absolute value of the initial surface potential under the negative pulse voltage is higher than that under the positive pulse voltage. So, the pulse voltage plays a more main role than DC voltage in charge accumulation.

5. Taking account of the pulse number effect, it is evident that the initial value rises with the pulse number increasing and then reaches saturation. Considering the decay rate characteristics, with the pulse number growing, the decay rate declines, and thus, the charge dissipates slowly. Also, the decay rate decreases in the following order: a negative DC voltage and a positive pulse voltage, a positive DC and a positive pulse voltage, a positive DC voltage and a negative pulse voltage and a negative DC and a negative pulse voltage.

Author details

Boxue Du

Address all correspondence to: duboxue@tju.edu.cn

School of Electrical Engineering and Automation, Tianjin University, Tianjin, China

References

[1] Xue Y, Zhang XP. Reactive power and AC voltage control of LCC HVDC system with controllable capacitors. IEEE Transactions on Power Systems. 2017;**32**(1):753–764.

[2] Qi B, Wei Z, Li CR. Creeping discharge of oil-pressboard insulation in AC-DC composite field: phenomenon and characteristics. IEEE Transactions on Dielectrics and Electrical Insulation. 2016;**23**(1):237–245.

[3] Murdiya F, Hanaoka R, Akiyama H, Miyagi K, Takamoto K, Kano T. Creeping discharge developing on vegetable-based oil/pressboard interface under AC voltage. IEEE Transactions on Dielectrics and Electrical Insulation. 2014;**21**(5):2102–2110.

[4] IEEE Guide for Loading Mineral-Oil-Immersed Transformers, IEEE Standard C57.91, 1995.

[5] Kole M, Dey TK. Role of interfacial layer and clustering on the effective thermal conductivity of CuO-gear oil nanofluids. Experimental Thermal and Fluid Science. 2011;**35**(7): 1490–1495.

[6] Keblinski P, Phillpot SR, Choi SUS, Eastman JA. Mechanisms of heat flow in suspensions of nano-sized particles (nanofluids). International Journal of Heat and Mass Transfer. 2001;**45**(4):855–863.

[7] Murshed SMS, Leong KC, Yang C. Determination of the effective thermal diffusivity of nanofluids by the double hot-wire technique. Journal of Physics D. 2006;**39**(24):5316–5322.

[8] Murshed SMS. Simultaneous measurement of thermal conductivity, thermal diffusivity, and specific heat of nanofluids. Heat Transfer Engineering. 2012;**33**(8):722–731.

[9] Rajab A, Sulaeman A, Sudirham S, Suwarno. A comparison of dielectric properties of palm oil with mineral and synthetic types insulating liquid under temperature variation. Institut Teknologi Bandung (ITB). Journal of Engineering and Technological Sciences. 2011;**42**(3):191–208.

[10] Li J, Zhang ZT, Zou P. Preparation of a vegetable oil-based nanofluid and investigation of its breakdown and dielectric properties. IEEE Electrical Insulation Magazine. 2012;**28**(5):43–50.

[11] Hwang JG, Zahn M, O'Sullivan FM, Pettersson LAA, Hjortstam O, Liu RS. Effects of nanoparticle charging on streamer development in transformer oil-based nanofluids. Journal of Applied Physics. 2010;**107**(1):1–17.

[12] J. Miao, M. Dong and L. P. Shen, "A Modified Electrical Conductivity Model for Insulating Oil-Based Nanofluids", IEEE International Conference on Condition Monitoring and Diagnosis (CMD), pp. 1126–1129, 2012.

[13] Tanaka T. Dielectric nanocomposites with insulating properties. IEEE Transactions on Dielectrics and Electrical Insulation. 2005;**12**(2):914–928.

[14] Smith RC, Liang C, Landry M, Nelson JK, Schadler LS. The mechanisms leading to the useful electrical properties of polymer nanodielectrics. IEEE Transactions on Dielectrics and Electrical Insulation. 2008;**15**(1):187–196.

[15] Jayaram S. Effects of thermal and viscous drag forces on AC breakdown characteristics of transformer oil. IEEE Conference on Electrical Insulation and Dielectric Phenomena (CEIDP); 1993. pp. 396–401.

[16] Kao KC. Theory of high-field electric conduction and breakdown in dielectric liquids. IEEE Transactions on Electrical Insulation. 1976;**11**(4):121–128.

[17] Vasheghani M, Marzbanrad E, Zamani C, Aminy M, Raissi B, Ebadzadeh T, Barzegar-Bafrooei H. Effect of Al_2O_3 phases on the enhancement of thermal conductivity and viscosity of nanofluids in engine oil. Heat Transfer Engineering. 2011;**47**(11):1401–1405.

[18] Timofeeva EV, Moravek MR, Singh D. Improving the heat transfer efficiency of synthetic oil with silica nanoparticles. Journal of Colloid and Interface Science. 2011;**364**(1):71–79.

[19] Putra N, Roetzel W, Das SK. Natural convection of nano-fluids. Heat and Mass Transfer. 2003;**39**(8–9):775–784.

[20] Jin HF, Andritsch T, Tsekmes IA, Kochetov R, Morshuis PHF, Smit JJ. Properties of mineral oil based silica nanofluids. IEEE Transactions on Dielectrics and Electrical Insulation. 2014;**21**(3):1100–1108.

[21] Wang FP, Xia ZF, Qiu Xl, Shen J, Zhang XP, An ZL. Piezoelectric properties and charge dynamics in poly(vinylidene fluoride-hexafluoropropylene) copolymer films with different content of HFP. IEEE Transactions on Dielectrics and Electrical Insulation. 2006;**13**(5):1132–1139.

[22] Tamura R, Miura Y, Watanabe T, Iahii T, Yamada N, Nitta T. Static electrification by forced oil flow in large power transformer. IEEE Transactions on Power Apparatus and Systems. 1980;**99**(1):335–343.

[23] Du BX, He ZY, Du Q, Guo YG. Effects of water absorption on surface charge and dielectric breakdown of polyimide/Al_2O_3 nanocomposite films. IEEE Transactions on Dielectrics and Electrical Insulation. 2016;**23**(1):134–141.

[24] Zhuang Y, Chen G, Chappell PH, Rotaru M. Surface potential decay: Effect of different corona charging times. IEEE Conference on Electrical Insulation and Dielectric Phenomena (CEIDP). 2012.620–623.

[25] Du BX, Li XL, Jiang JP. Surface charge accumulation and decay on direct-fluorinated oil-impregnated paper. IEEE Transactions on Dielectrics and Electrical Insulation. 2016;**23**(5):3094–3101.

[26] Zhang C, Shao T, Ma H, Zhang D, Ren C, Yan P, Tarasenko VF, Schamiloglu E. Experimental study on conduction current of positive nanosecond-pulse diffuse discharge at atmospheric pressure. IEEE Transactions on Dielectrics and Electrical Insulation. 2013;**20**(4):1304–1314.

[27] Simmons JG, Taylor GW, Tam MC. Thermally stimulated currents in semiconductors and insulators having arbitrary trap distributions. Physical Review B. 1973;**7**(8):3714–3719.

[28] Llovera P, Molinie P. New methodology for surface potential decay measurements: Application to study charge injection dynamics on polypropylene films. IEEE Transactions on Dielectrics and Electrical Insulation. 2012;**11**(6):1049–1056.

IntechOpen